BIOCELL
2021 45(2): 281-306

Tech Science Press

# Musk secretion in muskrats (*Ondatra zibethicus L.*): association with lipid and cholesterol metabolism-related pathways

Tianxiang ZHANG[1,#]; Meishan ZHANG[1,#]; Minghui SHI[1,#]; Weijiang JIN[1,#]; Shumiao ZHANG[2,#]; Mengyuan FAN[3]; Yimeng LI[1]; Yuping MENG[2]; Xuelin TIAN[4]; Shuqiang LIU[1,*]; Defu HU[1,*]

[1] School of Ecology and Nature Conservation, Beijing Forestry University, Beijing, 100083, China
[2] Beijing Milu Ecological Research Center, Beijing, 100083, China
[3] China Wildlife Conservation Association, Beijing, 100083, China
[4] Jining Academy of Agricultural Sciences, Jining, 272000, China

**Key words:** Muskrat, Scent gland, RNA-seq, Lipid, Cholesterol

**Abstract:** Male muskrats (*Ondatra zibethicus* L.) secrete musk from their scent glands during musk secretion season. Musk plays an important role as a communication pheromone during the breeding season. In this study, gas chromatography–mass spectrometry (GC–MS) was used to analyze the main components of musk. The GC–MS results after methyl esterification showed that 71.55% of the musk is composed of fatty acids. The other components of muskrat musk include cholesterol (9.31%) and other organics. Transcriptome comparison between musk secretion and non-secretion seasons showed significant changes in the scent glands for 53 genes involved in fatty acid and cholesterol synthesis and metabolism regulatory pathways, which include fatty acid biosynthesis, elongation, and metabolism; steroid biosynthesis; steroid hormone biosynthesis pathways. A reverse transcription–polymerase chain reaction analysis confirmed these detected changes. Overall, our results indicated that lipid synthesis and metabolism play important roles in musk compound synthesis by providing energy for musk production, and the produced musk provides a mechanism for male muskrats to communicate with females during the breeding season.

## Introduction

The muskrat (*Ondatra zibethicus L.*) is a rodent that lives in a semi-aquatic environment. Adult male muskrats have a pair of abdominal glands that secrete musk during the musk secretion season (April–May), which is also the breeding season for muskrats. Musk secreted by scented glands plays an important role in communication with females (van Dorp *et al.*, 1973). Male muskrats attract females during the breeding season by secreting this musk. These scent glands experience seasonal cyclical changes (Shereshkov *et al.*, 2006). During the musk secretion season, the glands swell, and secretion fills the glands. This secretion is a milky, viscous fluid that has a relatively strong scent (Zhang *et al.*, 2017). During the non-secretion season (October–February), the glands decrease in size (Chen *et al.*, 1996a) and do not secrete musk.

Previous chemical analyses showed that muskrat musk contains various components, such as fatty acids, esters, cholesterol, cyclic ketones, and alcohols (Chen *et al.*, 1996b, 1998). Different studies obtained varying results on the levels of lipids in muskrat musk. In 1994, Bao-Tang *et al.* (1994) employed gas chromatography–mass spectrometry (GC–MS) techniques to examine muskrat musk after methyl esterification, and found that it contained 12 different types of fatty acids, of which unsaturated fatty acids accounted for more than 60% of the fatty acid content. In 1998, Chen *et al.* (1998) employed GC–MS to analyze muskrat musk after methyl esterification, and found that it contained five types of fatty acids, which accounted for 50.98% of the musk composition, whereas cholesterol accounted for 7.21% of the musk composition. In 1998, Chen *et al.* (1998) employed GC–MS techniques and found six types of fatty acids, which accounted for 22.45% of the total content. In 2009, Zhao *et al.* (2009) employed GC–MS techniques and found that muskrat musk contained five types of fatty acids, which accounted for 29.5% of the musk composition. These

*Address correspondence to: Shuqiang Liu, liushuqiang@bjfu.edu.cn; Defu Hu, hudf@bjfu.edu.cn
#These authors contributed equally to this work
Received: 23 February 2020; Accepted: 12 May 2020

Doi: 10.32604/biocell.2021.010277

findings indicate that fatty acids are the main components of muskrat musk and that cholesterol may be one of the components. However, as there were differences in the sample processing methods and test conditions of these studies, muskrat musk fatty acid quantitation results showed variability. Alternatively, there are very few studies on the cholesterol content of muskrat musk. However, the regulatory mechanism of the synthesis of these components has remained unclear. Therefore, we studied the role of the lipid and steroid synthesis pathways in muskrat secretion using RNA sequencing (RNA-Seq) technology. These findings will provide a basis for understanding how musk is synthesized by muskrats during the musk secretion period.

The aforementioned studies showed that, during the musk secretion season, musk secreted by muskrats produce large amounts of fatty acids, cholesterol, and other substances. However, the synthesis mechanisms and functions of these components are still unclear. In this study, we applied GC–MS to quantify muskrat musk components and analyze lipid components. We combined RNA-Seq techniques to study gene expression changes in the lipid synthesis- and metabolism-related pathways. This study provides evidence that can help understand the synthesis mechanism of muskrat musk components.

## Materials and Methods

*Research animals*

In this study, all animals were treated in accordance with the National Animal Welfare Legislation, and all experimental procedures were carried out in accordance with the guidelines established by Beijing Forestry University. Six healthy adult male muskrats were purchased from a muskrat breeding center in Xinji City, Hebei Province. All muskrats were euthanized by aeroembolism (inject air into the vein to kill the animals) after anesthesia.

*Sample preparations*

Sampling of the scent glandular tissues was conducted on 7 November 2016 (during the non-secretion season), and sampling of both scent glandular tissues and secreted musk was conducted on 7 May 2017 (musk secretion season). The collected tissues were photographed and stored in liquid nitrogen for subsequent experimental analyses. The scent gland samples were dehydrated in an ethanol series and embedded in paraffin wax. Serial sections (4–6 μm) were mounted on slides coated with 3-aminopropyl-triethoxysilane (APES; ZSGB-BIO, Beijing, China). Some sections were stained with hematite hematoxylin (Solarbio, Beijing, China) for general histological observation.

*GC–MS analysis*

For the process of methyl esterification, 0.5 g of musk was weighed and dissolved in 5 mL of hexane. The solution was mixed for 10 min to make sure that it is completely dissolved, and 1 mL of 0.5 mol/L NaOH–$CH_3OH$ solution was added. Heat the mixture to 50°C after swaying for about 30 min to complete the methyl esterification process. To detect the components other than fatty acids, 50 mg of musk was dissolved in benzene and mixed with a whirlpool mixer at 4000 rpm/min for 1 min. The supernatant was placed in 5 mL flasks, from which 2-mL samples were extracted into vials, which were then placed in the GC–MS system to conduct measurements (Shimadzu, Kyoto, Japan).

GC–MS system parameters were as follows: DB-1 fused silica capillary column (28.0 m × 250.0 μm; 0.25 μm); pre-column pressure, 50 kPa (splitless injection); inlet temperature, 270°C; interface temperature, 280°C; temperature program: starting point at 100°C for 2 min, followed by increments of 6°C/min up to 280°C, and holding at 280°C for 10 min; carrier gas, He; injection volume, 1 μL; ionizing voltage, electronic ionization; ion source temperature, 250°C; gas flow rate, 1.0 mL/min; electron bombardment energy, 70 eV; electron multiplier voltage, 1.7 kV; and mass scan range, 20.0–400.0 amu. The results of the fragment ion analyses for the mass spectrum of each component were compared with the possible structure obtained from the National Institute of Standards and Technology library. The results were then combined with the retention time and data from previous studies to determine the musk components (Fan *et al.*, 2018).

*RNA extraction, library construction, and RNA-seq*

Total RNA of each scent gland tissue was isolated using Trizol reagent (Qiagen, Valencia, CA, USA), characterized on 1.8% agarose gel, and examined with a NanoDrop ND1000 spectrophotometer (NanoDrop Technologies, Wilmington, DE, USA). The total RNA of each sample was extracted using TRIzol reagent (Invitrogen, Carlsbad, CA, USA) following the manufacturer's instructions and treated with DNase I (Qiagen, Mississauga, Ontario, Canada). The quality and quantity of total RNA were analyzed using an Agilent 2100 Bioanalyzer (Agilent Technologies, CA, USA). The concentrations of total RNA were supposed to be more than 200 ng/μL, and the quantity should be more than 10 μg. RNA integrity was checked by agarose gel electrophoresis (1% agarose gel). Suitable RNA samples were selected for cDNA synthesis.

The RNA insert sizes of these samples were assessed using a Qubit 2.0 (Thermo Fisher Scientific Inc., Carlsbad, CA, USA) and Agilent 2100 Bioanalyzer (Santa Clara, CA, USA). The construction of the libraries and RNA-Seq were performed by the Biomarker Biotechnology Corporation (Beijing, China). mRNA was enriched and purified with Oligo(dT)-rich magnetic beads and then broken into short fragments with fragmentation buffer. Using these cleaved mRNA fragments as templates, first-strand cDNA was synthesized with random hexamers; then, buffer, deoxyribonucleotide triphosphates, RNase H, and DNA polymerase I, were added to synthesize second-strand cDNA. The resulting cDNAs were then purified by AMPure XP beads (Thermo Fisher Scientific Inc., Carlsbad, CA, USA). The purified cDNAs were then subjected to end-repair, and an overhang 'A' base was inserted at the 3' ends of the cDNA fragments. AMPure XP beads were used to select fragment sizes. Next, PCR amplification was performed to enrich the purified cDNA template. Finally, the six libraries were sequenced using an Illumina HiSeq™ 2500, which generated 100-nt paired-end reads.

*De novo transcriptome assembly and annotation*

After the clean reads were filtered from the raw reads, the reads were then assembled de novo using the Trinity platform (http://trinityrnaseq.sourceforge.net/). For each library, short reads were first assembled into longer contigs; then, components were generated using the overlap between the contigs. Finally, the components were identified using a De Bruijn graph and read information to obtain 22,680 unigenes. Unigenes were aligned to a series of protein databases using BLASTx (E-value ≤ 10−5), including the NCBI Nr, KEGG (http://www.genome.jp/kegg/kegg2.html), and GO (http://wego.genomics.org.cn/cgi-bin/wego/index.pl) databases. The deduced amino acid sequences of uni-transcripts were then compared with the Pfam (protein family) database using HMMER (E-value ≤ 10−10) to obtain unigene annotations.

*Expression annotation*

All usable reads were compared with each unigene using Bowtie (http://bowtie-bio.sourceforge.net/manual.shtml), then the expression level was estimated by RSEM (http://deweylab.github.io/RSEM/) according to the comparisons. Fragments Per Kilobase of transcript per Million mapped reads (FPKM) values were used to determine the expression abundance of each unigene.

*Quantitative real-time PCR*

From total RNA, first-strand cDNA was synthesized using gDNA and FastQuant RT Enzyme (FastQuant RT Kit with gDNA; Tiangen, Beijing, China). The 20-μL reaction mixture contained 260 ng of total RNA, 2 μL of 5× gDNA Buffer, 2 μL of 10× Fast RT Buffer, 1 μL of RT Enzyme Mix, and 2 μL of FQ-RT Primer Mix. The 25-μL PCR mixture contained 6 μL of first-strand cDNA, 1 μL of each primer, 12.5 μL of 2× Taq PCR Master Mix, and 4.5 μL of $ddH_2O$ (Tiangen, Beijing, China). The amplification process was as follows: 94°C for 3 min for the initial denaturation of the RNA/cDNA hybrid; 33 cycles of 94°C for 30 s, 55°C for 20 s, and 72°C for 20 s; and a final extension of 5 min at 72°C. The target genes are shown in Tab. S1. The glyceraldehyde-3-phosphate dehydrogenase cDNA fragment was amplified using the intron-spanning primers 5'-TTTGGCATCGTGGAAGGA-3' (bases 508–525) and 5'-CGAAGGTAGAAGAGTGGGAGT-3' (bases 892–872). The PCR products were electrophoresed in 1% agarose gel, and individual bands were visualized using ethidium bromide staining.

*Statistical analysis*

Results are presented as means ± standard error of the mean. To investigate any differences between the secretion and non-secretion seasons, we performed *t*-tests in Sigma Plot v. 12.5 (Li *et al.*, 2017); $0.01 < p < 0.05$ was considered significantly different; $0.001 < p < 0.01$ was considered highly significant. Unigene abundance differences between the samples were calculated using the Benjamini–Hochberg method based on the ratio of the FPKM values, and the false discovery rate (FDR) control method was used to identify the threshold of the *p*-value. Here, only unigenes with an absolute value of fold change ≥ 2 and FDR < 0.01 were used for subsequent analyses.

## Results

*Histology*

During the musk secretion season, the scent glands are dilated to an average length of 38.3 ± 3.97 mm. In contrast, during the non-secretion season, the glands show an average length of 15.3 ± 6.66 mm. The gland volume is significantly greater during the musk secretion season than during the non-secretion season ($p < 0.01$; Fig. 1a). The diameter of musk-secreting cells is significantly ($p < 0.01$) larger during the secretion season (13.93 ± 1.64 μm) than during the non-secretion season (5.45 ± 0.93 μm; Figs. 1b and 1c).

*Musk components*

The total ion chromatogram of muskrat musk GC–MS analysis reveals 16 main components aside from fatty acid, including cyclic ketones (41.98%), olefins (17.11%), esters (15.37%), and cholesterol (9.31%). After methyl esterification, the results reveal 48 components, of which 26 are fatty acids (71.55%) (Tabs. 1 and 2).

GC–MS results showed that fatty acids and cholesterol were both major components of muskrat musk, with methyl esterified fatty acids accounting for 71.55% (Tab. 1) and non-methyl esterified cholesterol accounting for 9.31% (Tab. 2) of muskrat musk.

*Transcriptome analysis*

The Illumina HiSeq 2500 high-throughput sequencing system was adopted to sequence the transcriptome of six samples of muskrat scent glands, which generated 27.84 Gb of clean data. Each sample produced 3.57 Gb of

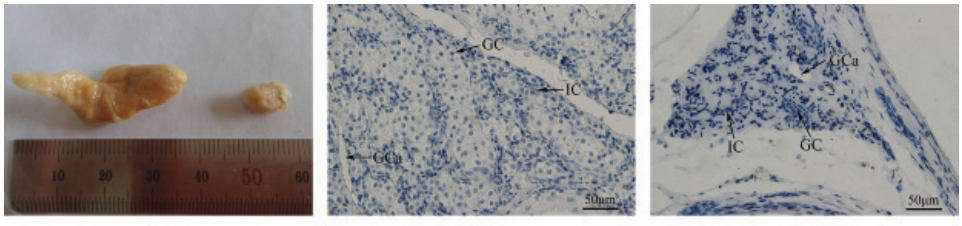


**FIGURE 1.** (a) An image of the muskrat scent glands during the secretion and non-secretion seasons. The volume of the scent gland is significantly higher in the secretion season than in the non-secretion season ($p < 0.01$). Left, secretion season; Right, non-secretion season. (b, c) Morphological sections in muskrat scent glands during the secretion and non-secretion seasons. The diameter of the secreting cells is significantly higher in the (b) secretion season than in the (c) non-secretion season ($p < 0.01$). Abbreviations: GC, glandular cells; IC, interstitial cells; GCa, glandular cavity. Scale bars represent 50 μm.

**TABLE 1**

**Identification of components of muskrat musk except for fatty acids by GC–MS**

| Name | Formula | Mol. weight | Area% |
|---|---|---|---|
| 1,5,9,13-Tetradecatetraene | $C_{14}H_{22}$ | 190 | 4.18 |
| Cyclopentadecanone | $C_{15}H_{28}O$ | 224 | 39.09 |
| Cyclopentadecanol | $C_{15}H_{30}O$ | 226 | 2.40 |
| Civetone | $C_{17}H_{30}O$ | 250 | 2.15 |
| 8-Cyclohexadecen-1-one | $C_{16}H_{28}O$ | 236 | 0.74 |
| 7-Tetradecenal, (7Z)- | $C_{14}H_{26}O$ | 210 | 1.03 |
| Glyceroltrielaidate | $C_{57}H_{104}O_6$ | 884 | 9.98 |
| 1,2-Dipalmitoyl-sn-glycerol | $C_{35}H_{68}O_5$ | 568 | 4.78 |
| 1,19-Eicosadiene | $C_{20}H_38$ | 278 | 0.56 |
| (Z)-9-Octadecen-1-ol | $C_{18}H_{36}O$ | 268 | 0.61 |
| Cholesta-3,5-diene | $C_{27}H_{44}$ | 368 | 12.36 |
| 8-Hexadecenal,14-methyl-, (8Z)- | $C_{17}H_{32}O$ | 252 | 3.92 |
| Cholesta-4, 6-dien-3-ol, (3.beta.)- | $C_{27}H_{44}O$ | 384 | 6.22 |
| 2-[[2-[(2-Ethylcyclopropyl)methyl]cyclopropyl] methyl]cyclopropaneoctanoic acid methyl ester | $C_{22}H_{38}O_2$ | 334 | 0.61 |
| Cholesterol | $C_{27}H_{46}O$ | 386 | 9.31 |
| Cholesta-4, 6-dien-3-one | $C_{27}H_{42}O$ | 382 | 2.06 |

clean data, of which Q30 bases accounted for at least 88.98%. Clean reads were assembled into a total of 14,917,239 contigs. As the length increased, the number of contigs decreased accordingly.

Database comparison provided functional annotation for all unigenes. We compared all the unigenes to the NCBI non-redundant (Nr) database using BLAST with an E-value cutoff ≤ 10−5 and a HMMER parameter E-value ≤ 10−10. As a result, a total of 22680 unigenes with annotated information were obtained. A total of 6013 unigenes were aligned to the COG database, which accounted for 26.51% of all unigenes; 13147 unigenes were aligned to the Gene Ontology (GO) database (57.97% of all unigenes); 9699 unigenes were aligned to the Kyoto Encyclopedia of Genes and Genomes (KEGG) database (42.76% of all unigenes); 13568 unigenes were aligned to the KOG database (59.82% of all unigenes); 16551 unigenes were aligned to the Swiss-Prot database (72.98% of all unigenes), and 22217 unigenes were aligned to the Nr database (97.96% of all unigenes).

RNA-Seq results for lipid synthesis and metabolism-related signaling pathways were as follows: fatty acid metabolism (ko00071; Fig. 2), steroid biosynthesis (ko00100; Fig. 3), citrate cycle (ko00020), fatty acid biosynthesis (ko00061), fatty acid elongation (ko00062), steroid hormone biosynthesis (ko00140), primary bile acid biosynthesis (ko00120), N-glycan biosynthesis (ko00510), glycerolipid metabolism (ko00561), and terpenoid backbone biosynthesis (ko00900) (all related pathways are shown in Fig. S1).

The expression changes of genes that regulate the fatty acid metabolic signaling pathways are shown in Tab. 3, the expression changes of genes that regulate the synthesis of cholesterol and related hormone signaling pathways are shown in Tab. 4, and the number of genes that showed significant expression changes in related pathways are shown in Tab. 5. The significant changes in gene expression levels ($p < 0.05$) during the musk secretion and non-secretion seasons are shown in Figs. 4 and 5. The changes ($p < 0.05$) in some of the gene expression levels of the scent glands during the musk secretion and non-secretion seasons are shown in Figs. 6 and 7.

*Quantitative real-time PCR results*

The RT-PCR results showed that genes with significant changes in expression in the ko00140, ko00900, ko00120, ko00510, ko00020, ko00061, ko00062, ko00071, and ko00561 pathways were detected in the muskrat scent glands. These changes were consistent with the gene expression changes detected in the transcriptome analysis (Figs. S2 and S3).

RNA-Seq results showed that the expression levels of seven genes in pathways related to fatty acid biosynthesis and fatty acid elongation (Fig. S1) underwent significant changes. Of these seven genes, six showed significant increases (Tabs. 3b and 3c; Figs. 4b, 4c, 5b and 5c). Expression levels of five genes related to cholesterol synthesis pathways (Fig. 3) significantly increased (Tab. 4a; Figs. 6a and 7a). The expression levels of many genes in the terpenoid backbone biosynthesis pathway, which is the precursor for cholesterol synthesis (Fig. S1), also significantly increased (Tab. 4e; Figs. 6e and 7e).

qRT-PCR demonstrated that changes in lipid biosynthesis- and metabolism-related gene expression are consistent with the transcriptome analysis results (Figs. S2 and S3), which verified the reliability of the RNA-Seq results.

**TABLE 2**

**Identification of fatty acids of muskrat musk by GC/MS after methyl esterification**

| Name | Formula | Mol. weight | Area% |
|---|---|---|---|
| cis-5-Dodecenoic acid | $C_{13}H_{24}O_2$ | 212 | 0.26 |
| Dodecanoic acid | $C_{13}H_{2}6O_2$ | 214 | 0.24 |
| 5-Octadecenoic acid | $C_{19}H_{36}O_2$ | 296 | 1.07 |
| Myristoleic acid | $C_{15}H_{28}O_2$ | 240 | 0.60 |
| Myristic-1-13C acid | $C_{15}H_{30}O_2$ | 242 | 0.78 |
| cis,cis-7, 10-Hexadecadienal | $C_{16}H_{28}O$ | 236 | 0.84 |
| Cyclopentadecanone | $C_{15}H_{28}O$ | 224 | 1.17 |
| cis-1, 2-Cyclododecanediol | $C_{12}H_{24}O_2$ | 200 | 0.27 |
| Palmitoleate | $C_{17}H_{32}O_2$ | 268 | 7.60 |
| Palmitic acid | $C_{17}H_{34}O_2$ | 270 | 4.26 |
| cis-9-Hexadecenoic acid | $C_{16}H_{30}O_2$ | 254 | 0.41 |
| cis-10-Heptadecenoic acid | $C_{18}H_{34}O_2$ | 282 | 0.27 |
| Cyclotridecanone | $C_{13}H_{24}O$ | 196 | 2.84 |
| Civetone | $C_{17}H_{30}O$ | 250 | 0.26 |
| Cyclohexane, 1, 2-diethenyl-4-(1-methylethylidene)-,cis- | $C_{13}H_{20}$ | 176 | 0.35 |
| 8, 11-Eicosadienoic acid | $C_{2}1H_{38}O_2$ | 322 | 1.74 |
| 11, 14-Eicosadienoic acid | $C_{21}H3_{8}O_2$ | 322 | 3.44 |
| 9-Octadecenoic acid, (E)- | $C_{19}H_{36}O_2$ | 296 | 4.89 |
| Oleic acid | $C_{19}H_{36}O_2$ | 296 | 3.87 |
| Stearic acid | $C_{19}H_{38}O_2$ | 298 | 1.38 |
| 5,11,14-Eicosatrienoate | $C_{21}H_{36}O_2$ | 320 | 0.98 |
| 5,13-Docosadienoate | $C_{23}H_{42}O_2$ | 350 | 8.67 |
| (Z)-9-Octadecen-1-ol | $C_{18}H_{36}O$ | 268 | 1.28 |
| Linoleic acid | $C_{19}H_{34}O_2$ | 294 | 0.51 |
| cis-13-Eicosenoic acid | $C_{21}H_{40}O_2$ | 324 | 3.48 |
| cis-11-Eicosenoic acid | $C_{21}H_{40}O_2$ | 324 | 5.41 |
| 18-Methylicosanoate | $C_{22}H_{44}O_2$ | 340 | 0.21 |
| 9,12-Octadecadien-1-ol,(9Z,12Z)- | $C_{18}H_{34}O$ | 266 | 3.87 |
| 18-Methylnonadecanoate | $C_{21}H_{42}O_2$ | 326 | 0.89 |
| 6,9-Octadecadienoic acid | $C_{19}H_{34}O_2$ | 294 | 0.27 |
| cis-10-Nonadecenoic acid | $C_{20}H_{38}O_2$ | 310 | 2.31 |
| Erucic acid | $C_{23}H_{44}O_2$ | 352 | 1.80 |
| Docosanoic acid | $C_{23}H_{46}O_2$ | 354 | 0.36 |
| 20-Methyl-docosanoate | $C_{24}H_{48}O_2$ | 368 | 0.28 |
| cis-13,16-Docasadienoic acid | $C_{23}H_{42}O_2$ | 350 | 3.19 |
| 9-(Z)-Octadecenoate | $C_{19}H_{36}O_2$ | 296 | 3.25 |
| Nervonic acid | $C_{25}H_{48}O_2$ | 380 | 3.10 |
| Tetracosanoic acid | $C_{25}H_{5}0O_2$ | 382 | 0.60 |
| Pentacosanoic acid | $C_{26}H_{52}O_2$ | 396 | 1.07 |
| cis-7,10,13,16-Docosatetraenoic acid | $C_{23}H_{38}O_2$ | 346 | 1.62 |
| Cholesterilene | $C_{27}H_{44}$ | 368 | 0.66 |
| Oleyl alcohol, acetate | $C_{20}H_{38}O_2$ | 310 | 11.47 |
| 19-Hexacosenoate | $C_{27}H_{52}O_2$ | 408 | 2.18 |

(Continued)

**Table 2 (continued).**

| Name | Formula | Mol. weight | Area% |
|---|---|---|---|
| Hexacosanoic acid | $C_{27}H_{54}O_2$ | 410 | 0.39 |
| 7-Octylidenebicyclo[4.1.0]heptane | $C_{15}H_{26}$ | 206 | 0.28 |
| 11-Hexacosyne | $C_{26}H_{50}$ | 362 | 2.25 |
| 24-Methyl-hexacosanoate | $C_{28}H_{56}O_2$ | 424 | 0.54 |
| Cholestane-3, 5-diol, 5-acetate, (3.beta., 5.alpha.)- | $C_{29}H_{50}O_3$ | 446 | 2.52 |

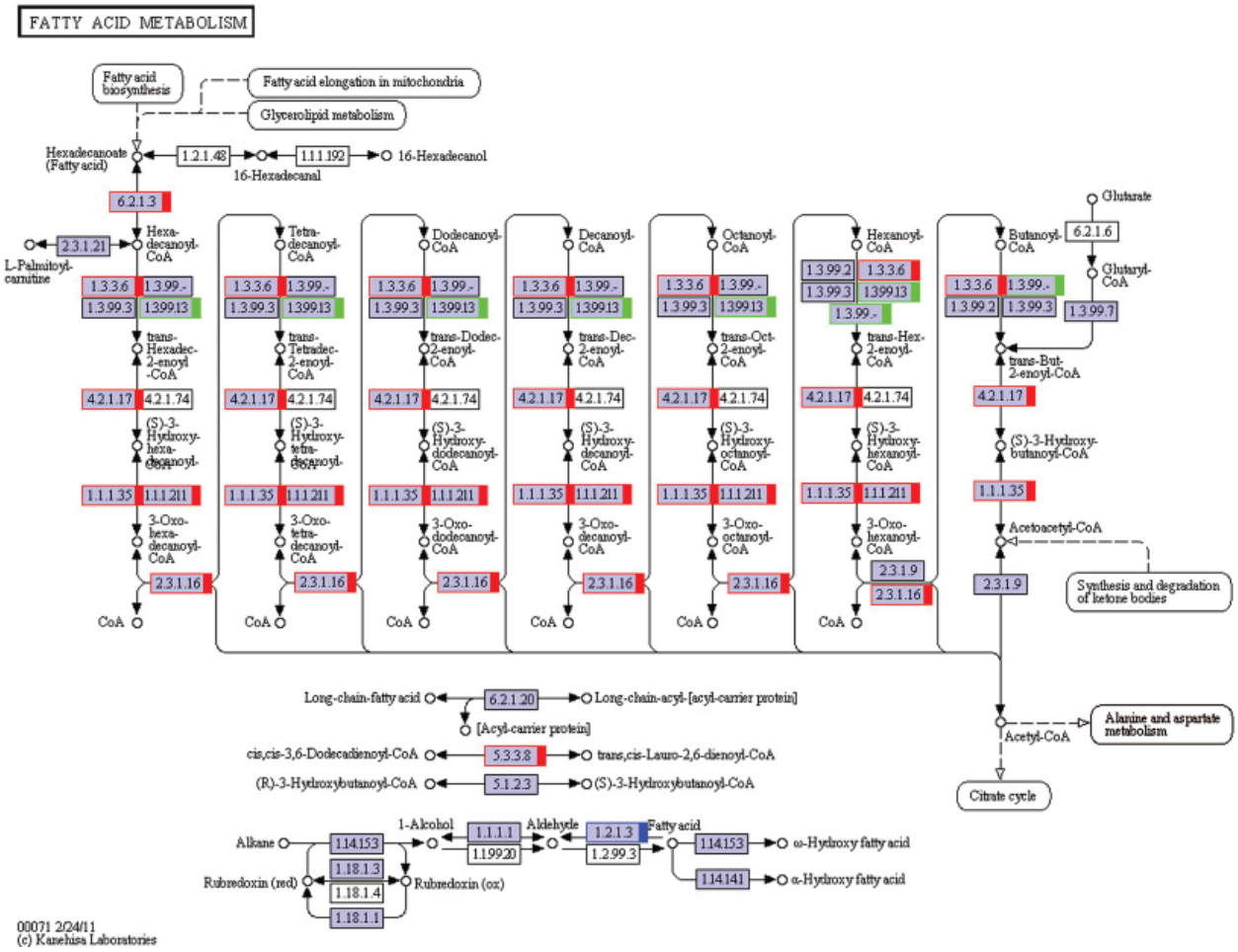


**FIGURE 2.** The KEGG pathway of fatty acid metabolism. The red marks show genes that are up-regulated, and the green ones show down-regulated. The blue one means some of the genes are up-regulated, and some are down-regulated. This KEGG pathway map is adapted here from http://www.kegg.jp/kegg/kegg1.html. The KEGG database has been described previously (Kanehisa and Goto, 2000; Kanehisa *et al.*, 2017, 2019).

## Discussion

The morphology results showed that, during the musk secretion season, muskrat scent gland size and glandular cell quantity were significantly greater than during the non-secretion season (Fig. 1), which is consistent with the findings of previous studies (Pushkala and Gupta, 2001; Zhang *et al.*, 2017). Different forms indicate differences in function, and the associated changes in morphology and function require further research.

The GC–MS results are consistent with those of Chen *et al.* (1998). RNA-Seq results showed that the gene expression levels in the pathways related to fatty acid biosynthesis and fatty acid elongation (Fig. S1), cholesterol synthesis pathways (Fig. 3), and the terpenoid backbone biosynthesis pathway (Fig. S1) underwent significant changes. From this, we suggest that these genes and metabolic pathways play important roles in the synthesis of major components of secreted muskrat musk. In addition, other studies have found that the musk fluid or musk secreted by Chinese forest musk deer, civet cats, and other musk-secreting animals also contains large amounts of fatty acids and cholesterol (Mookherjee *et al.*, 2004; Li *et al.*, 2016).

In the pathways that we hypothesized were relevant (Tab. 5), genes in the citrate cycle (TCA cycle), fatty acid biosynthesis, metabolism-related, steroid biosynthesis, and

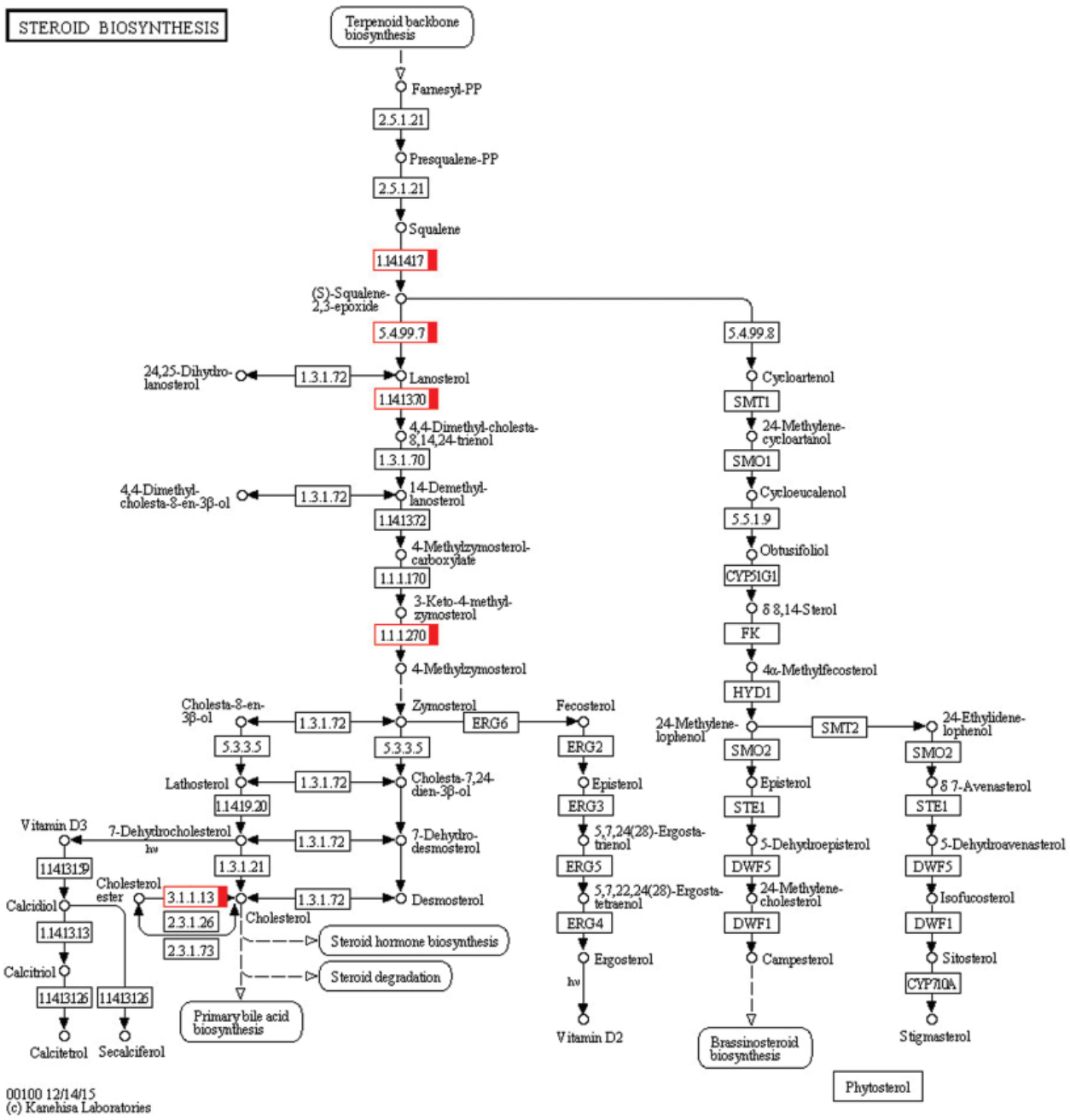


**FIGURE 3.** The KEGG pathway of steroid biosynthesis. The red marks show genes that are up-regulated. This KEGG pathway map is adapted here from http://www.kegg.jp/kegg/kegg1.html. The KEGG database has been described previously (Kanehisa and Goto, 2000; Kanehisa *et al.*, 2017, 2019).

terpenoid backbone biosynthesis pathways significantly changed. These pathways showed a similar trend that actively expressing during the musk secretion season.

Fatty acid biosynthesis can be divided into three steps: the de novo synthesis of saturated fatty acids, fatty acid carbon chain elongation, and unsaturated bond formation. During this process, fatty acid carbon chain elongation mainly occurs in the ER and mitochondria. In the ER, carbon-chain elongations are completed with fatty acyl-CoA as the starting point in a four-step cycle of condensation, reduction, dehydration, and re-reduction. Fatty acids are usually stored as triglycerides in organisms (Tvrdik *et al.*, 2000; Leonard *et al.*, 2004; Jakobsson *et al.*, 2006). RNA-Seq results showed that, in the glycerolipid (Fig. S1) metabolic pathway, fatty acid degradation (Fig. 2), and citrate cycle (Fig. S1), 23 genes showed significant changes in gene expression, of which 19 were significantly increased (Tabs. 3a, 3d and 3e; Figs. 4a, 4d, 4e, 5a, 5d, and 5e). Triglycerides are important energy storage material, and fatty acid degradation can release large amounts of energy (Cheung and Wong, 2008). Triglycerides can undergo hydrolysis to generate fatty acids and glycerol. Fatty acid oxidation is a catabolic reaction that produces $CO_2$ and $H_2O$ and can provide the organism with a large amount of energy. In animals, fatty acid catabolism occurs in mitochondria and peroxisomes (Zhang *et al.*, 2002). Fatty acids are converted to fatty acyl-CoA for β-oxidation. There are four β-oxidation steps: oxidation, hydration,

**TABLE 3**

**Transcript accumulation measurements of fatty acid metabolism-related genes involved in the muskrat musk secretion process**

| Unigene ID (EC name/annotation) | Regulated | $Log_2FC$ |
|---|---|---|
| **a. Citrate cycle (TCA cycle) (ko00020)-related genes** | | |
| c154234.graph_c0(2.3.3.8 /Acly) | Up | 1.65 |
| c181718.graph_c0(4.2.1.3/Aco1) | Up | 1.27 |
| c184117.graph_c2(1.1.1.42/Idh1) | Up | 2.30 |
| c189729.graph_c0(1.1.1.41/Idh3B) | Up | 1.30 |
| c154485.graph_c0(6.2.1.4/Sucla2) | Up | 1.35 |
| **b. Fatty acid biosynthesis (ko00061)-related genes** | | |
| c188079.graph_c1(6.4.1.2/Acacb) | Up | 2.97 |
| **c. Fatty acid elongation (ko00062)-related genes** | | |
| c100113.graph_c0(2.3.1.16/ACAA2) | Up | 2.26 |
| c154081.graph_c0(2.3.1.16/Acaa2) | Up | 2.46 |
| c154081.graph_c1(2.3.1.16/Acaa2) | Up | 2.95 |
| c176818.graph_c0(1.1.1.35/Hadh) | Up | 2.15 |
| c189709.graph_c0(4.2.1.17/Hadha) | Up | 1.58 |
| c187908.graph_c0(3.1.2.22/Ppt1) | Down | −1.38 |
| **d. Fatty acid degradation (ko00071)-related genes** | | |
| c186180.graph_c4(6.2.1.3/Acsl5) | Up | 2.25 |
| c166299.graph_c0(1.3.3.6/Acox3) | Up | 4.86 |
| c95056.graph_c0(1.3.8.8/Acadl) | Down | −1.52 |
| c177257.graph_c0(1.3.99.12/Acadsb) | Down | −1.89 |
| c189709.graph_c0(4.2.1.17/Hadha) | Up | 1.58 |
| c176818.graph_c0(1.1.1.35/Hadh) | Up | 2.15 |
| c100113.graph_c0(2.3.1.16/ACAA2) | Up | 2.26 |
| c154081.graph_c0(2.3.1.16/Acaa2) | Up | 2.46 |
| c154081.graph_c1(2.3.1.16/Acaa2) | Up | 2.95 |
| c189754.graph_c0(5.3.3.8/Eci1) | Up | 1.66 |
| c176790.graph_c0(5.3.3.8/Eci2) | Up | 8.76 |
| c186975.graph_c5(5.3.3.8/Eci2) | Up | 1.65 |
| c184675.graph_c1(1.2.1.3/Aldh3a2) | Up | 3.62 |
| c166519.graph_c0(1.2.1.3/Aldh2) | Down | −1.51 |
| c188162.graph_c0(1.2.1.36/Aldh1a1) | Down | −1.63 |
| **e. Glycerolipid metabolism (ko00561)-related genes** | | |
| c187137.graph_c0(3.1.1.23/Mgll) | Up | 1.53 |
| c185154.graph_c1(3.1.1.3/Pnpla3) | Up | 4.14 |
| c180403.graph_c0(2.3.1.20/DGAT1) | Up | 1.61 |

re-oxidation, and thiolysis. These four cyclic steps continue until all fatty acyl-CoA have become acetyl-CoA, which goes through the citrate cycle to produce $CO_2$ and a large amount of energy (Cheung and Wong, 2008). Musk secretion is a physiological activity that consumes large amounts of energy. During the musk secretion season, the provision of abundant fodder to muskrats can significantly increase the amount of musk secreted by muskrats (Chen, 1988; Huang, 1998). Studies have found that adiponectin plays an important regulatory role during musk secretion in muskrats (Zhang *et al.*, 2016) and causes a significant increase in the activity of intracellular mitochondria in muskrat scent gland cells, during the musk secretion season (Chen *et al.*, 1996b; Chen, 2007). Therefore, we propose that fatty acid oxidation and related metabolic pathways produce large amounts of energy that are required for muskrat musk secretion.

Cholesterol is a small lipid molecule that serves an important physiological role in organisms. It is a precursor

**TABLE 4**

**Transcript accumulation measurements of cholesterol biosynthesis-related genes involved in the muskrat musk secretion process**

| Unigene ID (EC name/annotation) | Regulated | $Log_2FC$ |
|---|---|---|
| **a. Steroid biosynthesis (ko00100)-related genes** | | |
| c166709.graph_c0(1.14.14.17/Sqle) | Up | 2.42 |
| c148945.graph_c0(5.4.99.7/Lss) | Up | 3.30 |
| c142879.graph_c0(1.14.13.70/Cyp51) | Up | 2.08 |
| c147614.graph_c2(3.1.1.13/Lipa) | Up | 1.54 |
| c172106.graph_c1(1.1.1.62/Hsd17b7) | Up | 3.97 |
| **b. Primary bile acid biosynthesis (ko00120)-related genes** | | |
| c184362.graph_c0(1.1.1.181/Hsd3b7) | Up | 1.97 |
| c154780.graph_c0(5.1.99.4/Amacr) | Up | 3.09 |
| c179794.graph_c1(1.17.99.3/Acox2) | Up | 7.07 |
| c188694.graph_c3(1.1.1.35/Hsd17b4) | Up | 4.97 |
| c174928.graph_c0(2.3.1.176/Scp2) | Up | 5.81 |
| **c. Steroid hormone biosynthesis (ko00140)-related genes** | | |
| c189834.graph_c0(2.8.2.2/Sult2b1) | Up | 2.58 |
| c149099.graph_c0(1.14.14.19/Cyp17a1) | Up | 4.17 |
| c97465.graph_c0(1.1.1.146/Hsd11b1) | Up | 2.77 |
| c179490.graph_c0(1.14.14.1/Cyp1a1) | Up | 5.82 |
| c177279.graph_c0(1.3.1.22/Srd5a3) | Down | −2.16 |
| c156542.graph_c0(2.4.1.17/Ugt1a6a) | Down | −1.83 |
| **d. N-Glycan biosynthesis (ko00510)-related genes** | | |
| c95502.graph_c0(2.4.1.259/Alg9) | Up | 1.51 |
| c154819.graph_c0(3.2.1.113/Man1b1) | Up | 1.68 |
| c183448.graph_c0(3.2.1.113/Man1a2) | Up | 1.86 |
| c182710.graph_c0(3.2.1.113/Man1c1) | Down | −2.84 |
| c185766.graph_c0(3.2.1.113/MAN1A1) | Down | −2.02 |
| c188645.graph_c0(3.2.1.114/Man2a1) | Down | −1.34 |
| c186296.graph_c0(2.4.99.1/St6gal1) | Down | −1.71 |
| **e. Terpenoid backbone biosynthesis (ko00900)-related genes** | | |
| c166351.graph_c0(2.3.3.10/HMGCS1) | Up | 2.35 |
| c119784.graph_c0(1.1.1.34/Hmgcr) | Up | 2.40 |
| c119745.graph_c0(4.1.1.33/Mvd) | Up | 3.17 |
| c178880.graph_c1(2.5.1.87/Dhdds) | Up | 2.75 |
| c176644.graph_c0(2.5.1.91/Pdss2) | Up | 3.15 |

for the synthesis of many bioactive molecules, such as bile acid and steroid hormones (Hanukoglu, 1992; Liu and Song, 2013). Cholesterol synthesis is mostly based on the acetyl-CoA in the cytosol, which, under enzyme catalysis, sequentially becomes terpenoids, such as mevalonate, isoprene units, squalene, and lanosterol. After the removal of three carbons, cholesterol is formed (Zhang *et al.*, 2002). Steroid hormones include hormones from the adrenal cortex and sex hormones, which are secreted from the adrenal cortex and gonads (Pushkala and Gupta, 2001). Different enzymes can then stimulate cholesterol to produce different bioactive molecules. Bile acids are the major end-product of cholesterol metabolism in the body and can assist in lipid absorption and transport, and promote fatty acid oxidation (Davis, 2007; Russell, 2009). As noted above, fatty acid metabolism provides large amounts of energy for musk secretion in muskrats. As an important regulatory factor in fatty acid metabolism, primary bile acids play an important role in musk secretion. Transcriptome results showed that the expression levels of five genes in the primary bile acid biosynthesis pathway (Fig. S1) showed significant increases (Tab. 4b; Figs. 6b and 7b). These findings showed that this pathway is enhanced during the musk

**TABLE 5**

**The amount of genes that showed significant changes in expression between the secretion and non-secretion seasons in related pathways**

| Name of pathways | The amount of up-regulated genes | The amount of down-regulated genes |
|---|---|---|
| Citrate cycle (TCA cycle) | 5 | 0 |
| Fatty acid biosynthesis | 1 | 0 |
| Fatty acid elongation | 5 | 1 |
| Fatty acid degradation | 11 | 4 |
| Glycerolipid metabolism | 3 | 0 |
| Steroid biosynthesis | 5 | 0 |
| Primary bile acid biosynthesis | 5 | 0 |
| Steroid hormone biosynthesis | 4 | 2 |
| N-Glycan biosynthesis | 3 | 4 |
| Terpenoid backbone biosynthesis | 5 | 0 |

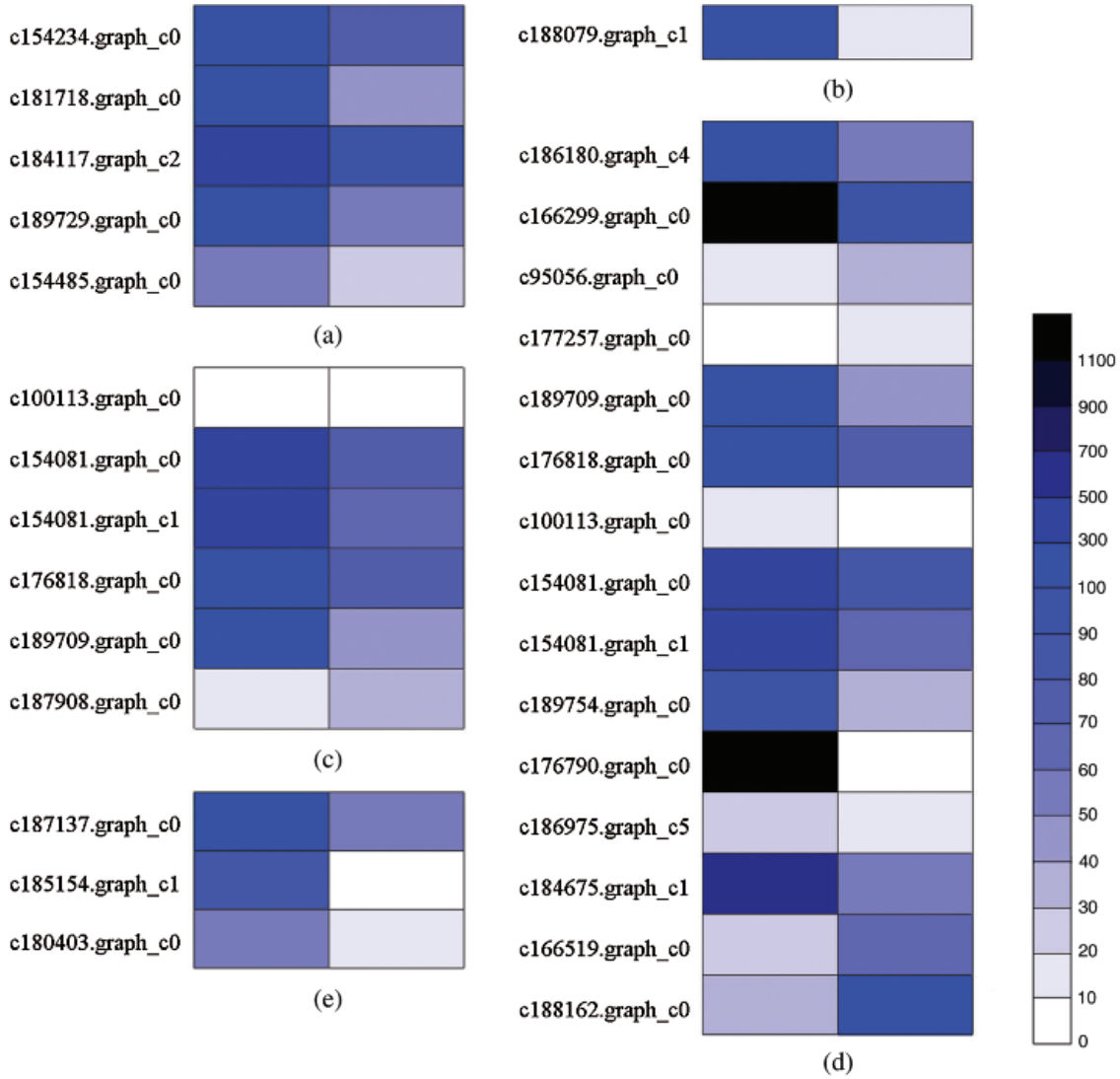


**FIGURE 4.** Transcript accumulation measurements of fatty acid metabolism-related genes involved in the muskrat musk secretion process. The ID of each enzyme name and expression is indicated above. The expression of each uni-transcript is shown on two grids, with the left one representing the FPKM values in the secretion season, and the right one representing the FPKM value in the non-secretion season. The grids with sixteen different color scale levels show the absolute expression magnitude of secretion seasons, with the FPKM values 0–10, 10–20, 20–30, 30–40, 40–50, 50–60, 60–70, 70–80, 80–90, 90–100, 100–300, 300–500, 500–700, 700–900, 900–1100, and over 1100 represented by color scale levels 1–16, respectively (FDR < 0.01, FC ≥ 2). (a) Citrate cycle (TCA cycle), (b) fatty acid biosynthesis, (c) fatty acid elongation, (d) fatty acid degradation, (e) glycerolipid metabolism.

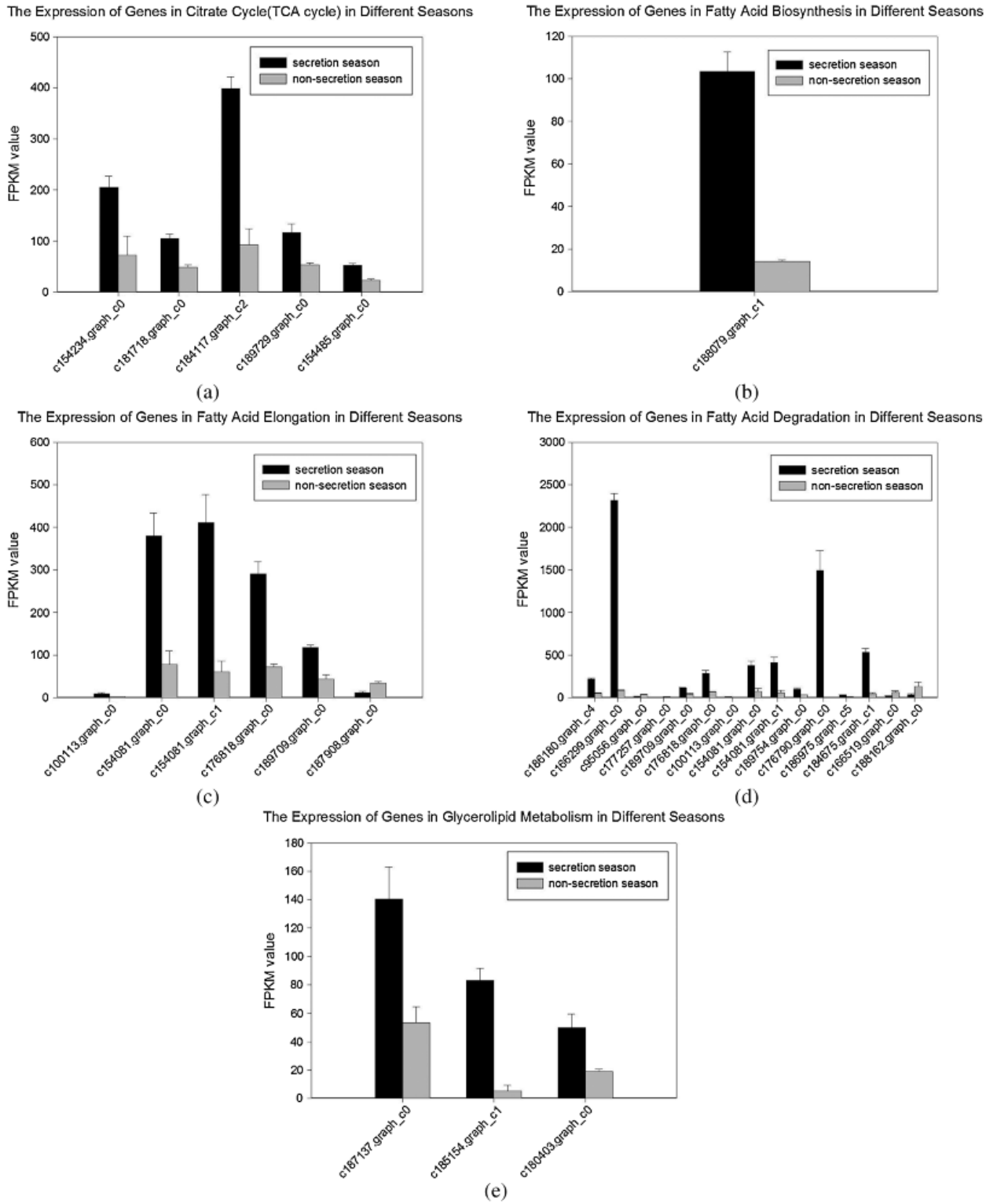


**FIGURE 5.** Transcript accumulation measurements of fatty acid metabolism-related genes involved in the muskrat musk secretion process (FDR < 0.01, FC ≥ 2). (a) Citrate cycle (TCA cycle), (b) fatty acid biosynthesis, (c) fatty acid elongation, (d) fatty acid degradation, (e) glycerolipid metabolism.

secretion season compared with during the non-secretion season, and the increase in primary bile acid synthesis supported this hypothesis.

A study showed that steroid hormones are an important factor for scent gland development and secreting musk (Li *et al.*, 2011). Previous experimental results have revealed that muskrat scent gland cells have the ability to self-synthesize male hormones, and the autocrine and paracrine secretions of sex hormones jointly regulate musk secretion (Han *et al.*, 2017). The transcriptomics results showed that the expression levels of six genes in the steroid hormone biosynthesis pathway (Fig. S1) showed significant changes, of which four were significantly increased (Tab. 4c; Figs. 6 and 7c). These

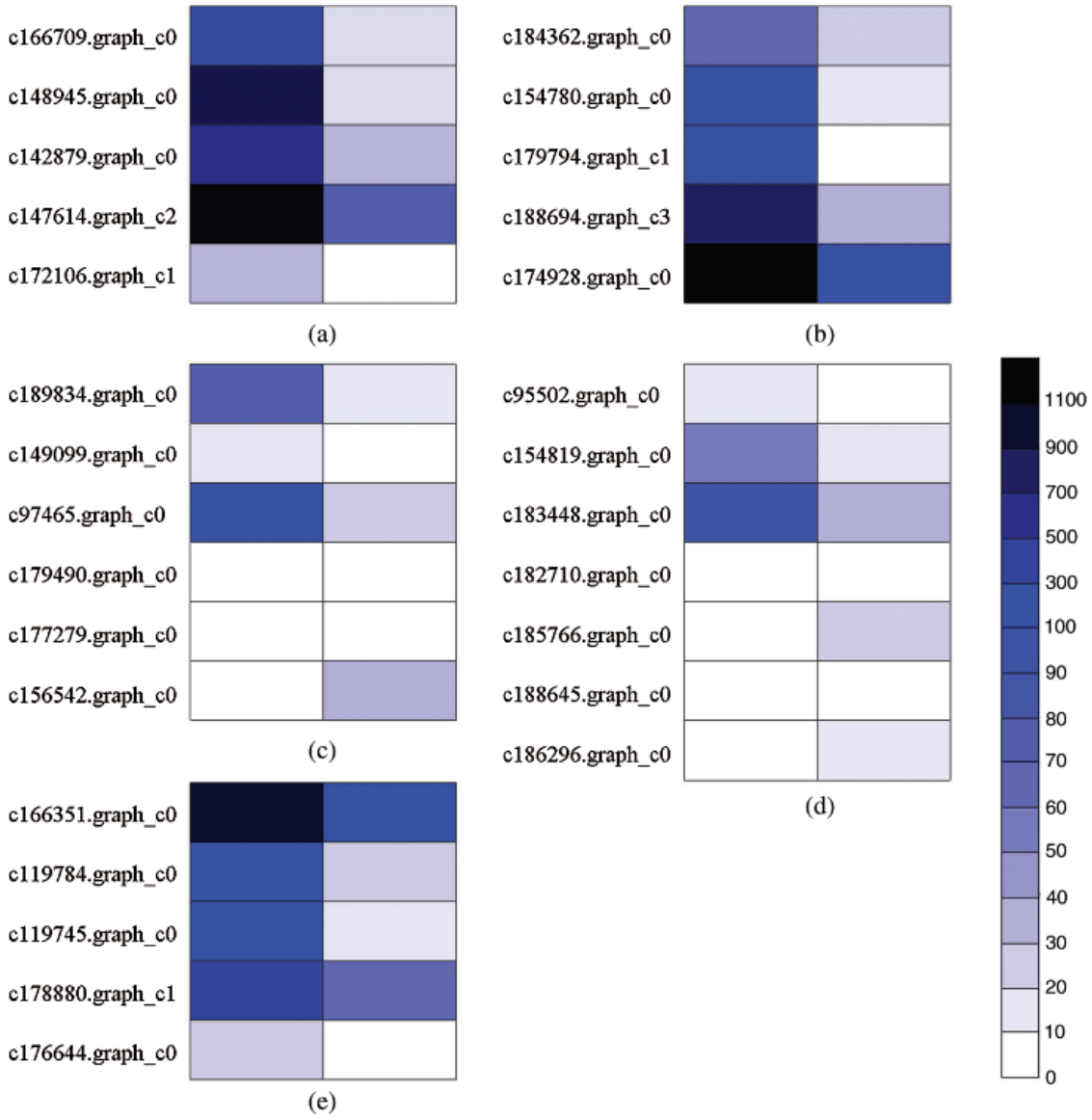


**FIGURE 6.** Transcript accumulation measurements of cholesterol biosynthesis-related genes involved in the muskrat musk secretion process. The ID of each enzyme name and expression pattern is indicated above. The expression pattern of each uni-transcript is shown on two grids, with the left one representing the FPKM values in the secretion seasons, and the right one representing the FPKM value in the non-secretion season. The grids with sixteen different grayscale levels show the absolute expression magnitude of secretion seasons, with the RPKM values 0–10, 10–20, 20–30, 30–40, 40–50, 50–60, 60–70, 70–80, 80–90, 90–100, 100–300, 300–500, 500–700, 700–900, 900–1100, and over 1100 represented by grayscale levels 1–16, respectively (FDR < 0.01, FC ≥ 2). (a) Steroid biosynthesis, (b) primary bile acid biosynthesis (c), steroid hormone biosynthesis, (d) N-glycan biosynthesis, (e) terpenoid backbone biosynthesis.

results are consistent with the hypothesis that muskrat scent gland cells can carry out the autocrine secretion of sex hormones, and the expression levels of many crucial genes involved in steroid hormone synthesis are significantly increased during musk secretion season. Our transcriptomic results provide an important basis for studying the autocrine steroid hormones secreted by muskrat scent glands that regulate musk secretion.

In animals, terpenoids can be used for N-glycan synthesis in addition to cholesterol synthesis (Cheung and Wong, 2008). However, there are seven genes in the N-glycan biosynthesis pathway (Fig. S1) that showed significant changes, of which three were significantly increased (Tab. 4d; Figs. 6d and 7d). These results showed that the N-glycan synthesis pathway in muskrats, compared with the cholesterol synthesis pathway, may not play a substantial role during the musk secretion season.

Recent studies have found that the levels of cytokines such as adiponectin, which regulate lipid metabolism, are significantly increased during the musk secretion season, and jointly participate in regulating musk secretion. This research applies GC–MS and RNA-Seq techniques to study the functions of lipid biosynthesis and metabolism regulation in muskrat musk secretion. Gene expression in lipid and steroid biosynthesis pathways provide the main components of musk during musk secretion season. Musk is an important pheromone that males use to attract and communicate with females. During the mating season, musk production and secretion requires a lot of energy. Gene expression in the lipid metabolic

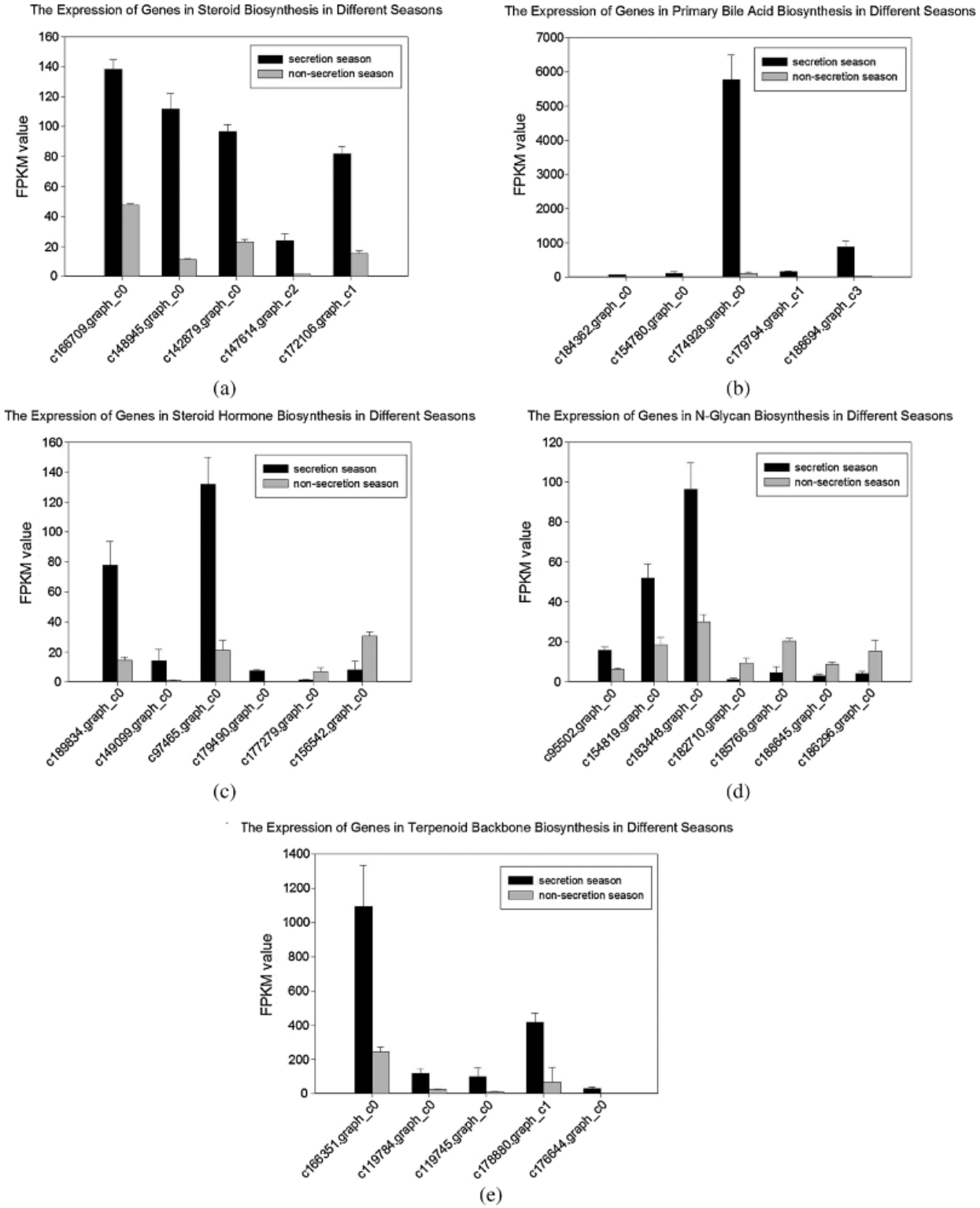


**FIGURE 7.** Transcript accumulation measurements of cholesterol biosynthesis-related genes involved in the muskrat musk secretion process (FDR < 0.01, FC ≥ 2). (a) Steroid biosynthesis, (b) primary bile acid biosynthesis, (c) steroid hormone biosynthesis, (d) N-glycan biosynthesis, (e) terpenoid backbone biosynthesis.

pathway provides the energy to support this important physiological process. Musk components and secretion regulation are complex issues, and there is still a substantial amount that is unknown about this unique physiological phenomenon.

**Acknowledgement:** The experimental facilities were provided by the School of Ecology and Nature Conservation Innovation Laboratory, Beijing Forestry University. We thank Mallory Eckstut, Ph.D., from Liwen Bianji, Edanz Editing China (www.liwenbianji.cn/ac), for editing the English text of a draft of this manuscript.

**Data Availability Statement:** The data used to support the findings of this study are available from the corresponding author upon request.

**Funding Statement:** This work was supported by Beijing Municipal Natural Science Foundation (Grant No. 5202016) and Fundamental research funds for the central universities (Grant No. 2019YC18).

**Conflicts of Interest:** The authors declare that they have no conflicts of interest to report regarding the present study.

## References

Li BT, Li CS, (1994). Determination of chemical composition of muskrat musk. *Chinese Pharmaceutical Journal* **29**: 396–397.

Chen J, Liu Z, Song F, Liu S (1998). Analysis of chemical constitutes in lipid from musk-rat musk by gas chromatography/mass spectrometry. *Chinese Journal of Analytical Chemistry* **26**: 1142–1145.

Chen Y, Jin S, Tong Y, Qao XH, Zhou A, Erzhen XU, Liu C, Wu YJ (1996a). Studies on morphology of cystgland and histological structure in the periods of secreting fragrant of muskrat. *Acta Theriologica Sinica* **16**: 151–154.

Chen Y, Tong Y, Gao X, Wei H, Li ZK, Wang C (1996b). A preliminary study on the scent gland development and the collection of scent secret in living musk rats. *Acta Theriologica Sinica* **16**: 43–47.

Chen YS (1988). Comparative studies on the pharmacological activities of muskrat and musk. *Zhong Yao Tong Bao* **13**: 46–48.

Chen YS (2007). Histological observation on musk-secreting scented gland in Muskrat. *Chinese Journal of Zoology* **42**: 91–95.

Cheung HY, Wong CYA (2008). *Essential Biochemistry: For Multidisciplinary Learning.*. vol. 6, pp. 344-367. Mcgraw Hill, Singapore.

Davis DM (2007). Cholestasis and endogenous opioids. *Clinical Pharmacokinetics* **46**: 825–850. DOI 10.2165/00003088-200746100-00002.

van Dorp DA, Klok R, Nugteren DH (1973). New macrocyclic compounds from the secretions of the civet cat and the musk rat. *Chemischer Informationsdienst* **4**: 915–928.

Fan M, Zhang M, Shi M, Zhang T, Qi L, Yu J, Li X, Lin S, Huang Z, Yang S, Zhou J, Li Y, Sun X, Cha M, Xu S, Liu Y, Guo X, Hu D, Liu S (2018). Sex hormones play roles in determining musk composition during the early stages of musk secretion by musk deer (*Moschus berezovskii*). *Endocrine Journal* **65**: 1111–1120. DOI 10.1507/endocrj.EJ18-0211.

Han W, Xie W, Zhang Y, Zhang F, Zhang H, Han Y, Yuan Z, Weng Q (2017). Seasonal expression of P450c17 and 5α-reductase-2 in the scented gland of male muskrats (*Ondatra zibethicus*). *General and Comparative Endocrinology* **254**: 60–67. DOI 10.1016/j.ygcen.2017.09.015.

Hanukoglu I (1992). Steroidogenic enzymes: Structure, function, and role in regulation of steroid hormone biosynthesis. *Journal of Steroid Biochemistry and Molecular Biology* **43**: 779–783. DOI 10.1016/0960-0760(92)90307-5.

Huang BJ (1998). Nutrition influence on musk secretion of breeding musk deer. *Zoological Research* **19**: 296–300.

Jakobsson A, Westerberg R, Jacobsson A (2006). Fatty acid elongases in mammals: their regulation and roles in metabolism. *Progress in Lipid Research* **45**: 237–249. DOI 10.1016/j.plipres.2006.01.004.

Kanehisa M, Furumichi M, Tanabe M, Sato Y, Morishima K (2017). KEGG: new perspectives on genomes, pathways, diseases and drugs. *Nucleic Acids Research* **45**: D353–D361. DOI 10.1093/nar/gkw1092.

Kanehisa M, Goto S (2000). KEGG: kyoto encyclopedia of genes and genomes. *Nucleic Acids Research* **28**: 27–30. DOI 10.1093/nar/28.1.27.

Kanehisa M, Sato Y, Furumichi M, Morishima K, Tanabe M (2019). New approach for understanding genome variations in KEGG. *Nucleic Acids Research* **47**: D590–D595. DOI 10.1093/nar/gky962.

Leonard AE, Pereira SL, Sprecher H, Huang YS (2004). Elongation of long-chain fatty acids. *Progress in Lipid Research* **43**: 36–54. DOI 10.1016/S0163-7827(03)00040-7.

Li D, Chen B, Zhang L, Gaur U, Ma T, Jie H, Zhao G, Wu N, Xu Z, Xu H, Yao Y, Lian T, Fan X, Yang D, Yang M, Zhu Q, Satkoski Trask J (2016). The musk chemical composition and microbiota of Chinese forest musk deer males. *Scientific Reports* **6**: 18975. DOI 10.1038/srep18975.

Li Q, Weng J, Zhang H, Lu L, Ma X, Wang Q, Cao H, Liu S, Xu M, Weng Q (2011). Immunohistochemical evidence: testicular and scented glandular androgen synthesis in muskrats (*Ondatra zibethicus*) during the breeding season. *European Journal of Histochemistry* **55**: e32. DOI 10.4081/ejh.2011.e32.

Li Y, Zhang T, Zhou J, Yang S, Fan M, Sun X, Zhang M, Xu S, Cha M, Hu X, Qi L, Lin S, Liu S, Hu D, Buratti E (2017). Transcriptome analysis of muskrat scented glands degeneration mechanism. *PLoS One* **12**: e0176935. DOI 10.1371/journal.pone.0176935.

Liu T, Song B (2013). Mechanisms of negative feedback regulation of cholesterol biosynthesis. *Chinese Journal of Cell Biology* **35**: 401–409.

Mookherjee BD, Narula APS, Monteleone MG, Trenkle RW (2004). Macrocylic musk composition, organoleptic uses thereof and process for preparing same, **10**: 401–424. *http://www.freepatentsonline.com/6720303.html*.

Pushkala K, Gupta PD (2001). Steroid hormones regulate programmed cell death: a review. *Cytobios* **106**: 201–217.

Russell DW (2009). Fifty years of advances in bile acid synthesis and metabolism. *Journal of Lipid Research* **50**: S120–S125. DOI 10.1194/jlr.R800026-JLR200.

Shereshkov VI, Shumilova TE, Kuzmin DA, Yanvareva IN, Nozdrachev AD (2006). Effects of hypoxic factors on cardiac chronotropic reactions in the muskrat *Ondatra zibethicus* in free behavior. *Journal of Evolutionary Biochemistry and Physiology* **42**: 461–468. DOI 10.1134/S0022093006040120.

Tvrdik P, Westerberg R, Silve S, Asadi A, Jakobsson A, Cannon B, Loison G, Jacobsson A (2000). Role of a new mammalian gene family in the biosynthesis of very long chain fatty acids and sphingolipids. *Journal of Cell Biology* **149**: 707–718. DOI 10.1083/jcb.149.3.707.

Zhang J, Campbell RE, Ting AY, Tsien RY (2002). Creating new fluorescent probes for cell biology. *Nature Reviews Molecular Cell Biology* **3**: 906–918. DOI 10.1038/nrm976.

Zhang T, Li W, Qi L, Fan M, Shen J, Wang Y, Wang W, Hu X, Cai R, Zhou R, Wei Y, Zhou J, Yang S, Hu D, Liu S (2016). Adiponectin plays a role in energy metabolism for musk secretion in scent glands of muskrats (*Ondatra zibethicus*). *Endocrine Journal* **63**: 633–641. DOI 10.1507/endocrj.EJ15-0720.

Zhang T, Peng D, Qi L, Li W, Fan M, Shen J, Yang L, Wang Y, Wang W, Hu X (2017). Musk gland seasonal development and musk secretion are regulated by the testis in muskrat (*Ondatra zibethicus*). *Biological Research* **50**: 1–9. DOI 10.1186/s40659-016-0106-3.

Zhao WG, Chen YS, Zhao M, Li XW, Liu DY (2009). Study on the comparison for the muskrat perfume secretion of fragrant gland cell cultured in vitro and that in nature. *Special Wild Economic Animal & Plant Research* **4**: 50–53.

## Supplementary Section

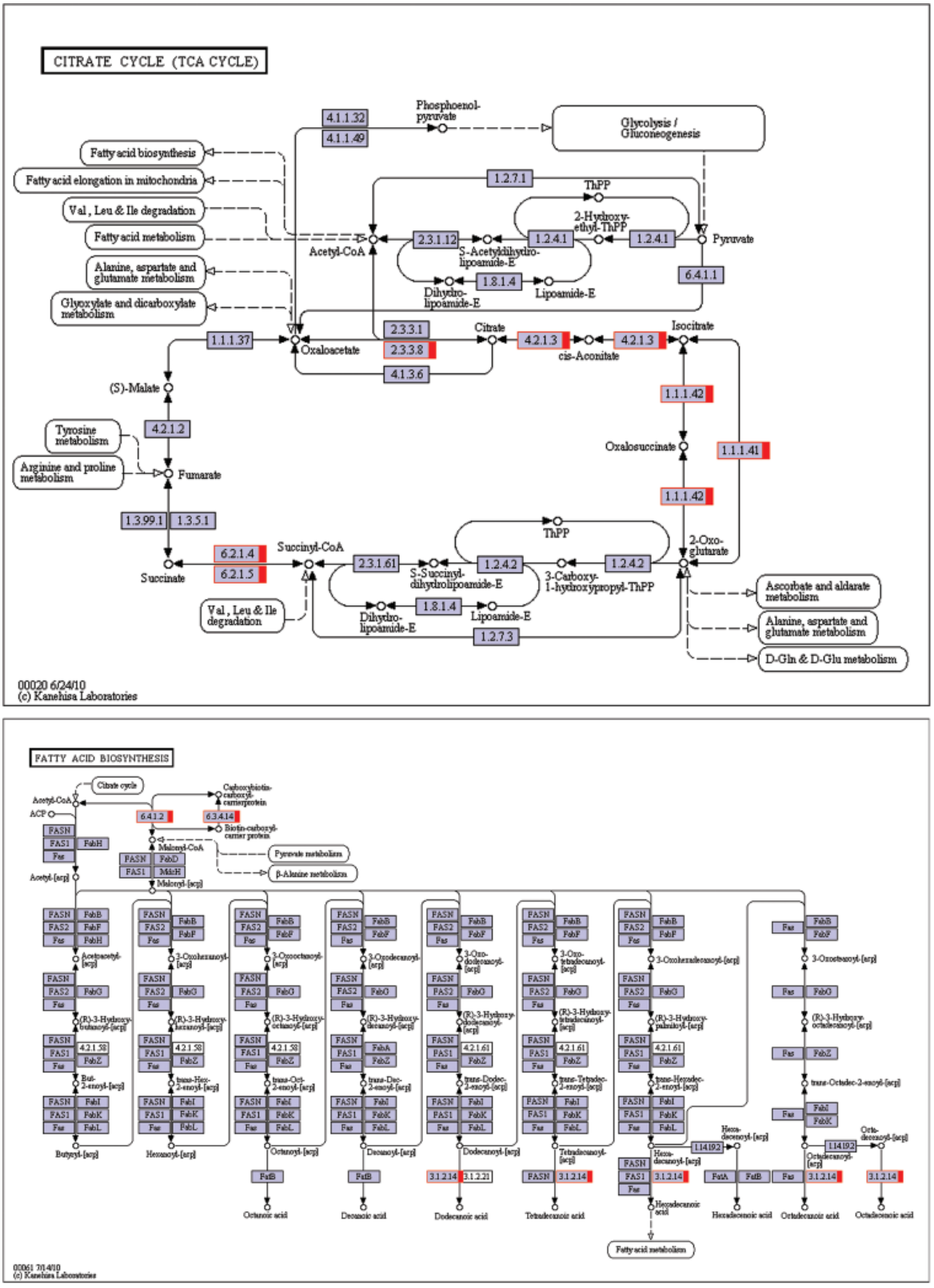


**FIGURE S1.** (continued)

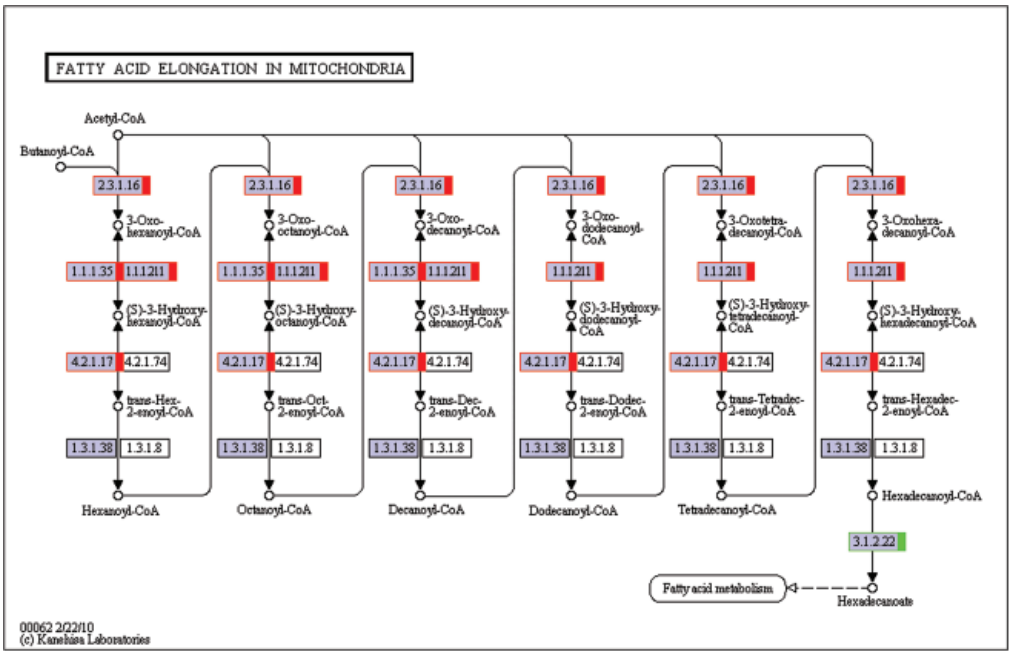


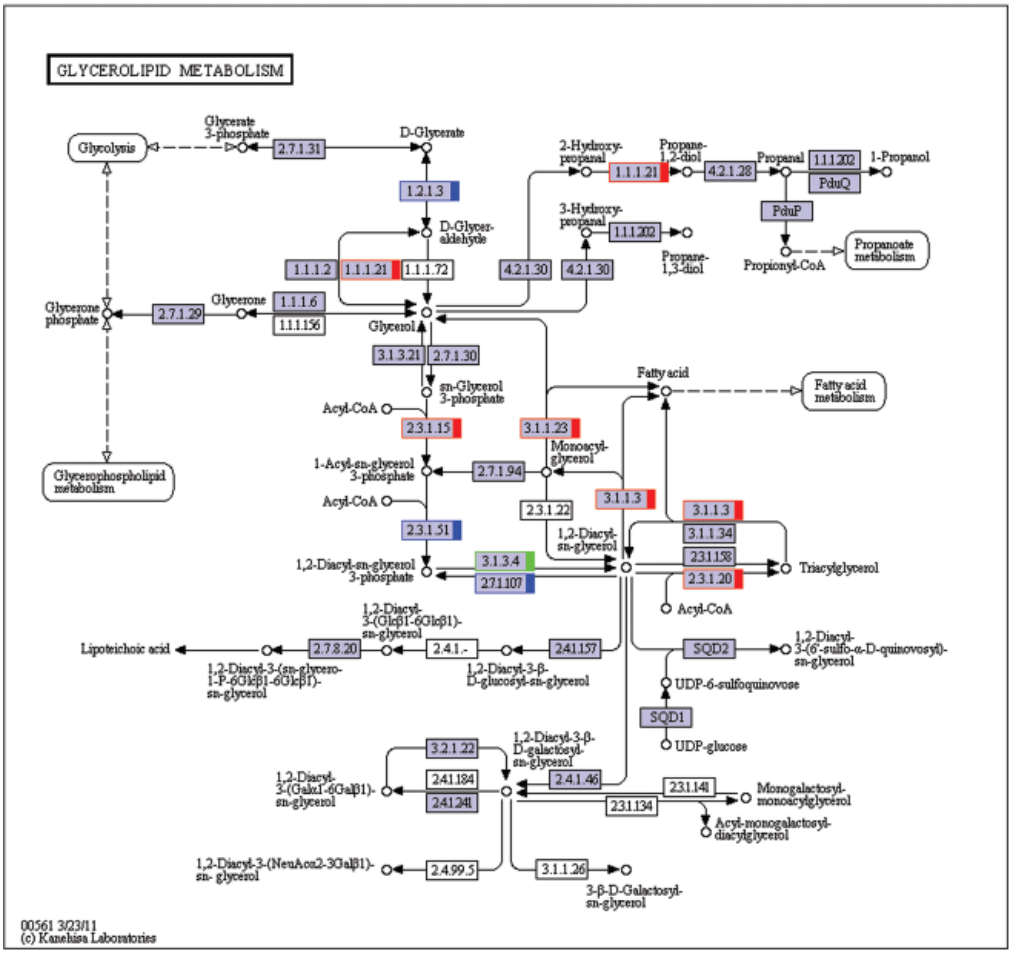


**FIGURE S1.** (continued)

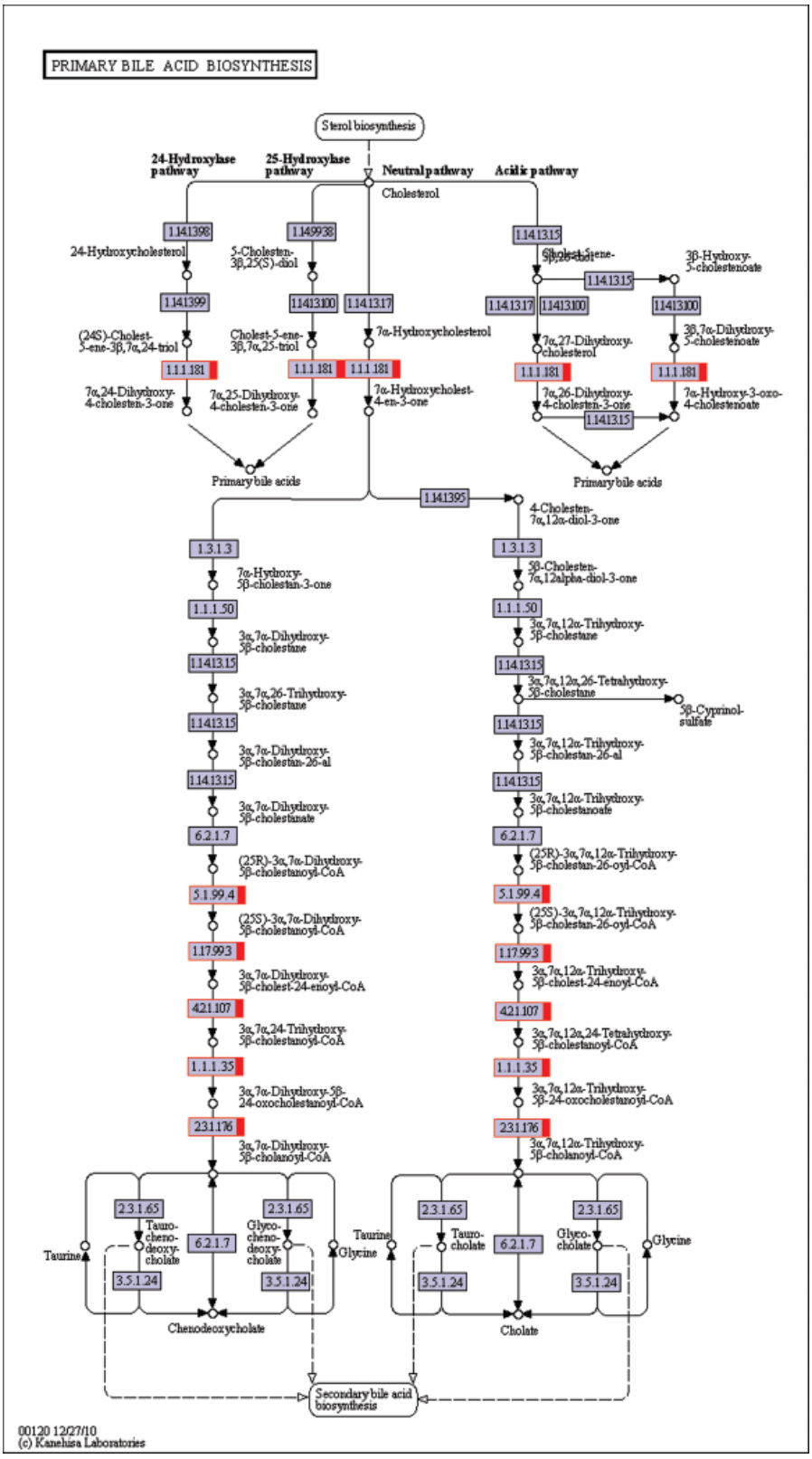


**FIGURE S1.** (continued)

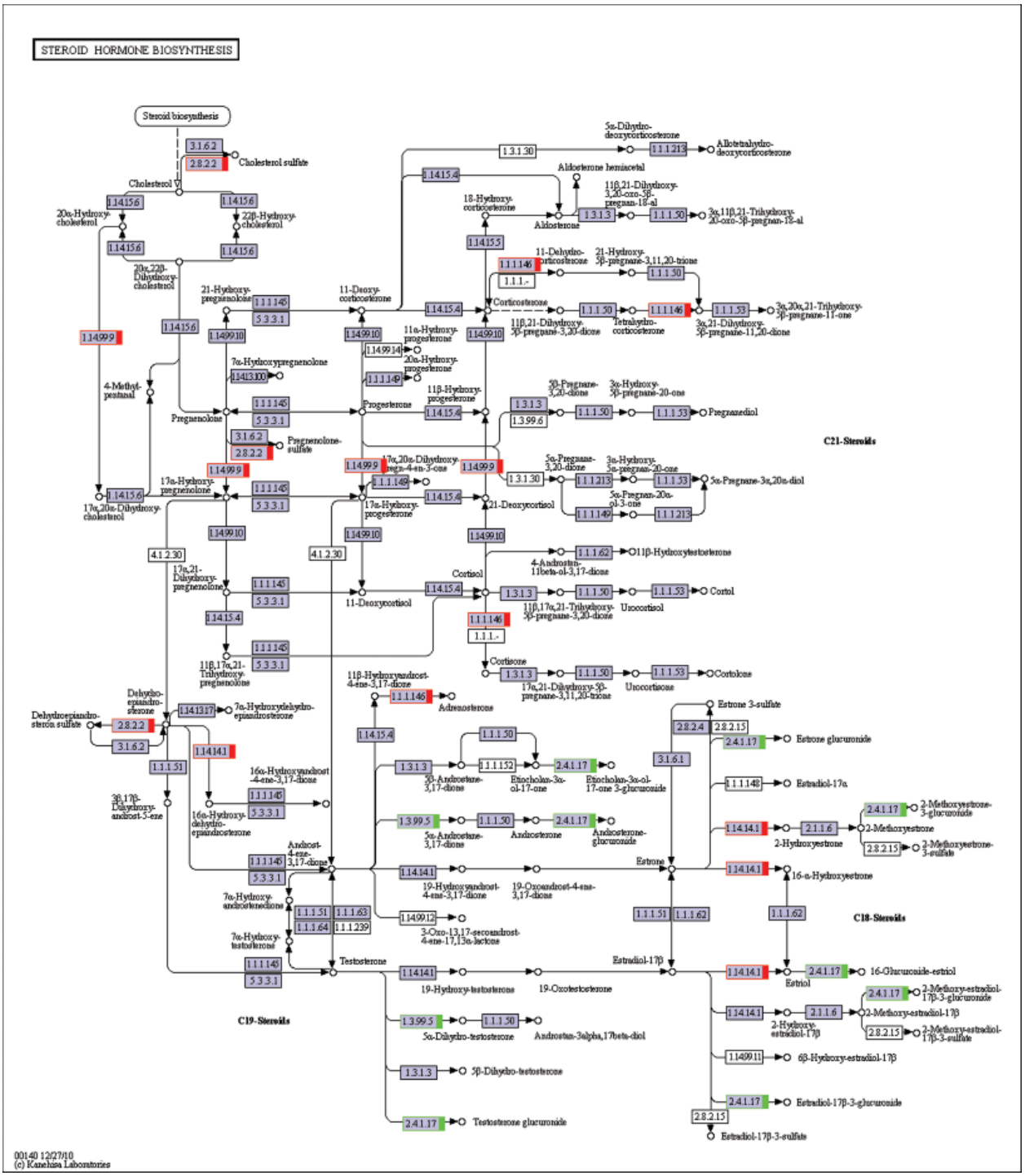


**FIGURE S1.** (continued)

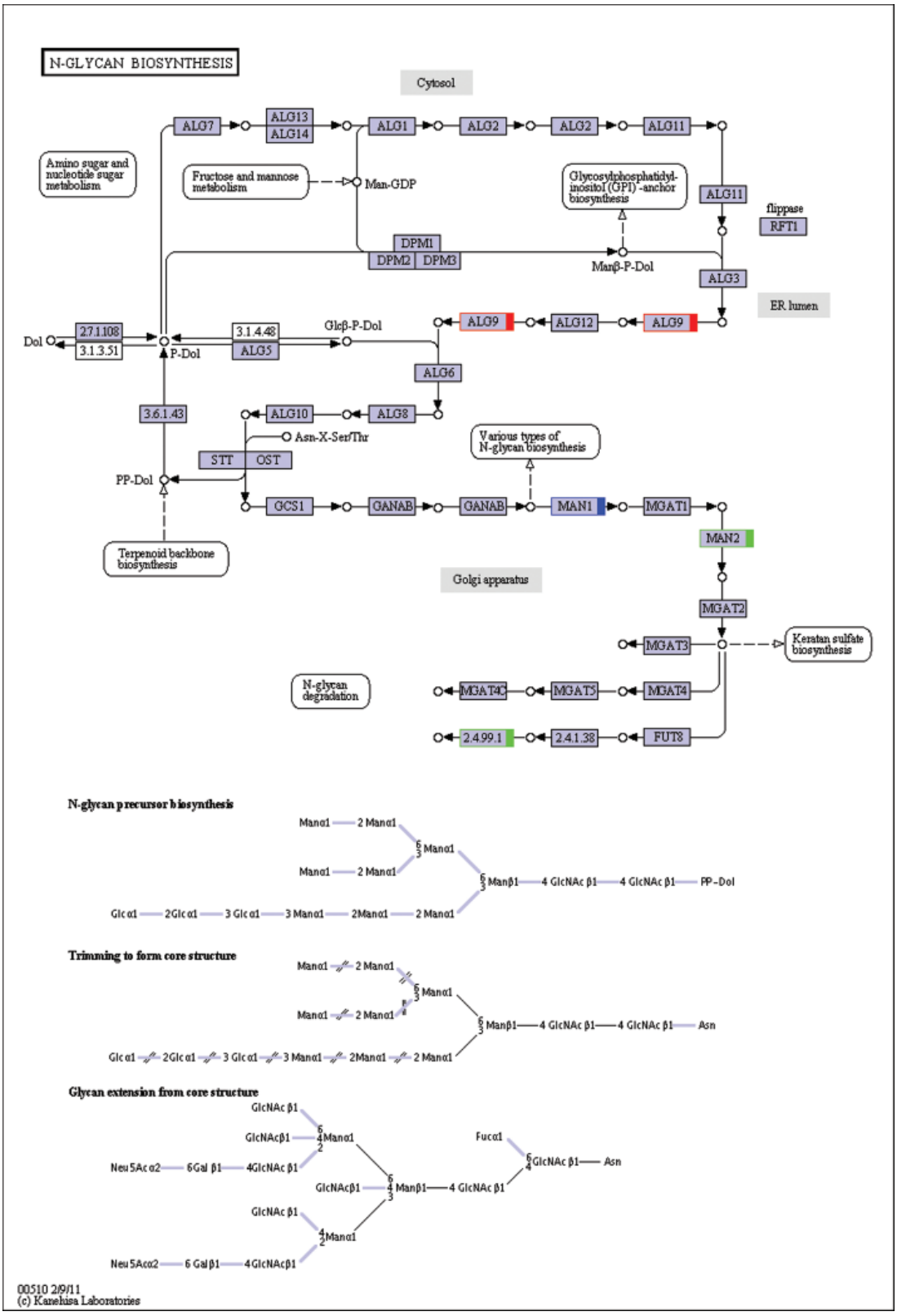


**FIGURE S1.** (continued)

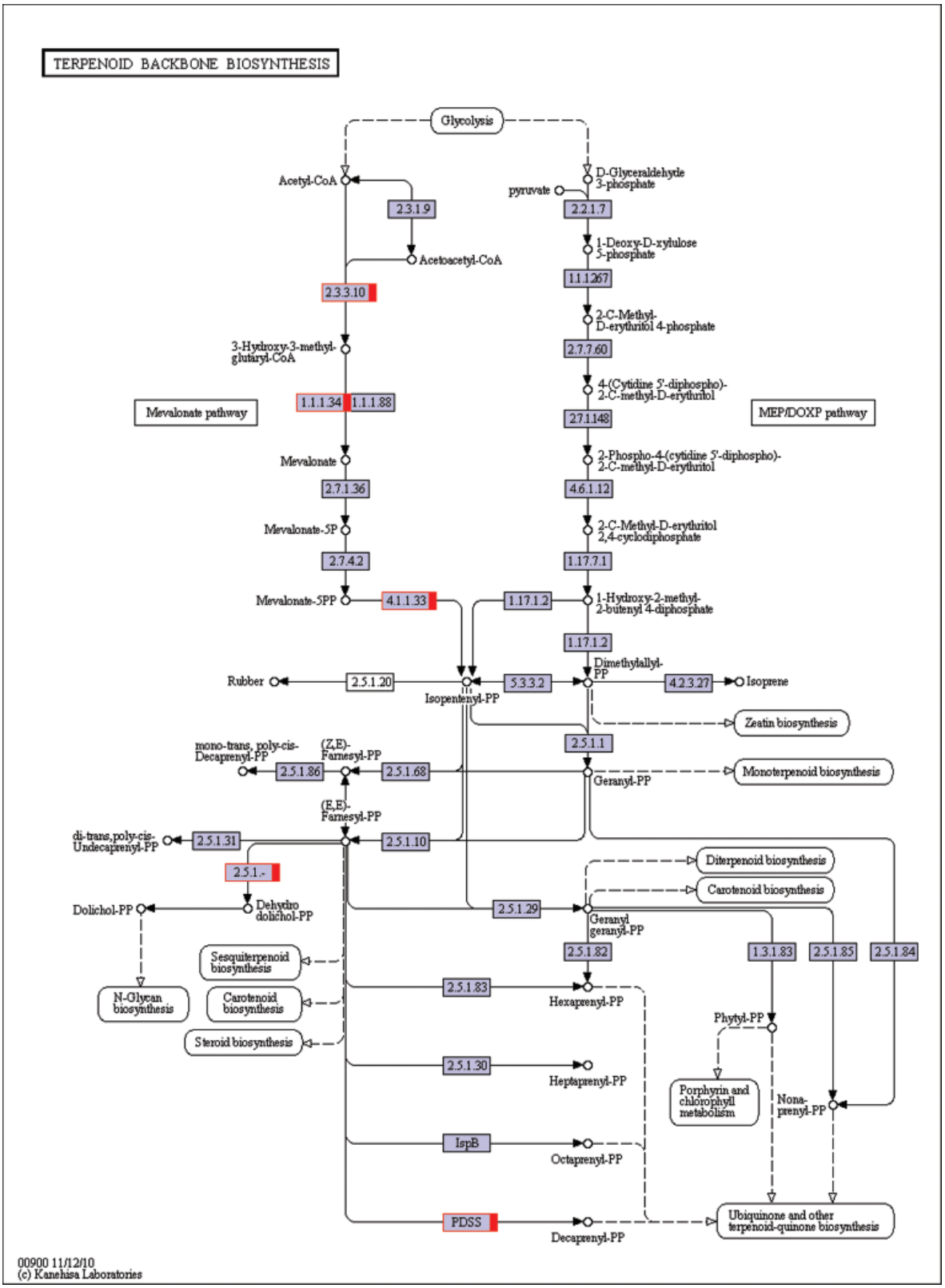


**FIGURE S1.** KEGG reference mappings for citrate cycle (TCA cycle), fatty acid biosynthesis, fatty acid elongation, glycerolipid metabolism, primary bile acid biosynthesis, steroid hormone biosynthesis, N-glycan biosynthesis and terpenoid backbone biosynthesis pathways. The red marks shows genes that are up regulated and the green ones shows down regulated. The blue one means some of the genes are up regulated and some are down regulated.

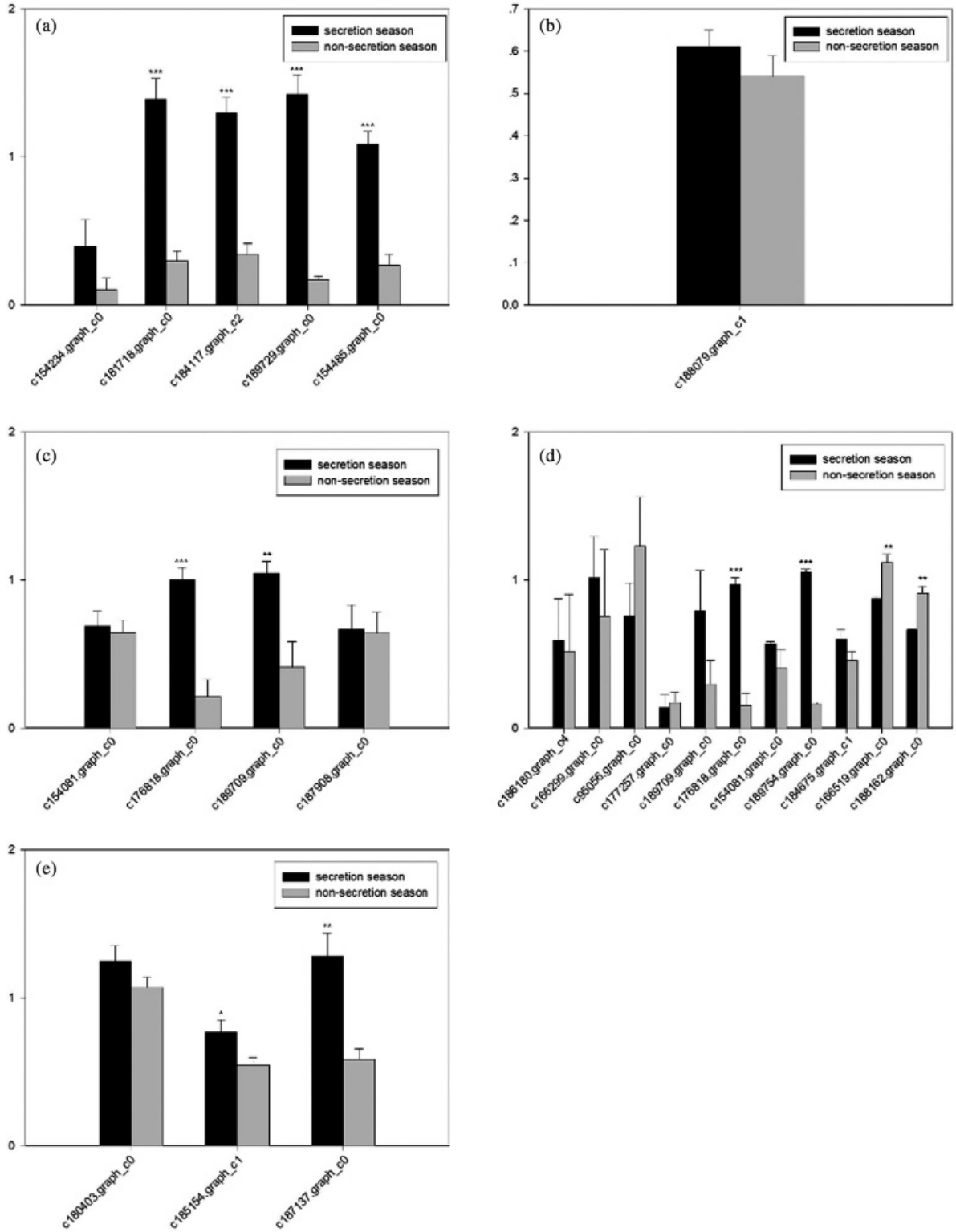


**FIGURE S2.** Grey scale measurements of fatty acid metabolism-related genes and GAPDH in the scent gland by RT-RCR. Data are presented as the mean ± SEM from at least three independent experiments, and error bars indicate SEM; *, ** and *** Denote statistically significant differences between secretion and non-secretion seasons (*, $0.01 < p < 0.05$; **, $0.001 < p < 0.01$, ***, $p < 0.001$). (a) Citrate cycle (TCA cycle); (b) Fatty acid biosynthesis; (c) Fatty acid elongation; (d) Fatty acid degradation; (e) Glycerolipid metabolism.

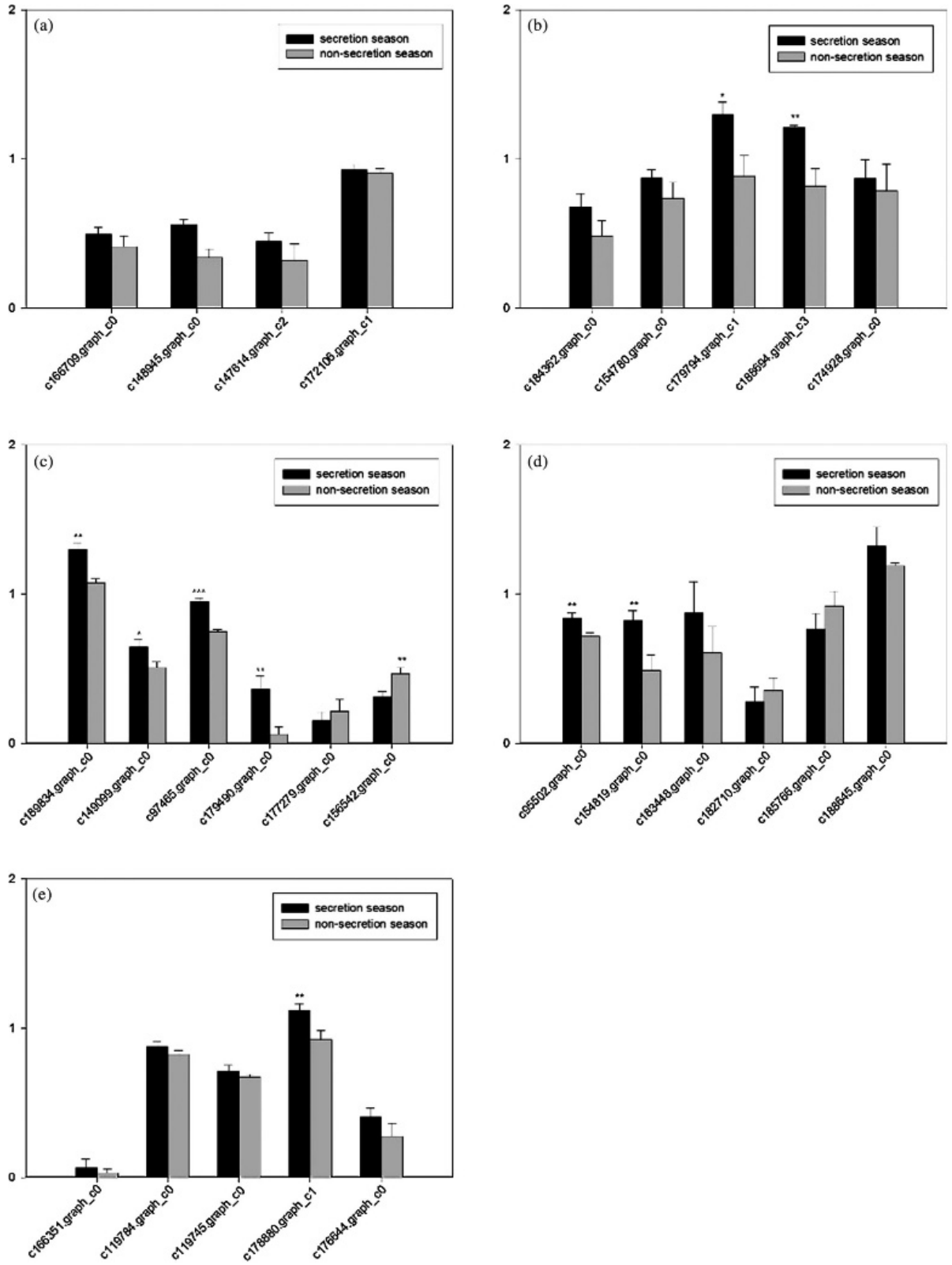


**FIGURE S3.** Grey scale measurements of cholesterol biosynthesis-related genes and GAPDH in the scent gland by RT-RCR. Data are presented as the mean ± SEM from at least three independent experiments, and error bars indicate SEM; *, ** and *** Denote statistically significant differences between secretion and non-secretion seasons (*, $0.01 < p < 0.05$; **, $0.001 < p < 0.01$, ***, $p < 0.001$). (a) Steroid biosynthesis; (b) Primary bile acid biosynthesis; (c) Steroid hormone biosynthesis; (d) N-Glycan biosynthesis; (e) Terpenoid backbone biosynthesis.

## TABLE S1

### List of relative uni-transcripts in lipid biosynthesis and metabolic regulatory pathways in muskrat scented gland

| #ID | Expression in secretion season | Expression in non-secretion season | STDEV of the secretion result | STDEV of the non-secretion result | log2FC | regulated | Length | KEGG_annotation | nr_annotation | Forward primer sequence (5'–3') | Reverse primer sequence (5'–3') |
|---|---|---|---|---|---|---|---|---|---|---|---|
| c188079.graph_c1 | 103.52 | 14.35 | 0.57 | 9.14 | 2.97 | up | 8202 | K11262\|0.0\|mmu:100705\|Acacb, AI597064, AW743042, Acc2, Accb | acetyl-CoA carboxylase 2 | CTGTGGTGACTGGACGAGC | TGGCGAAGATGATGAGGG |
| c100113.graph_c0 | 9.30 | 2.22 | 0.44 | 2.11 | 2.26 | up | – | K07508\|1e-15\|ptr:455414\|ACAA2 | phosphatidylinositol 4,5-bisphosphate 5-phosphatase A isoform X1 | – | – |
| c154081.graph_c0 | 379.90 | 78.25 | 31.34 | 53.42 | 2.46 | up | 1136 | K07508\|0.0\|mmu:52538\|Acaa2, 0610011L04Rik, AI255831, AI265397, D18Ertd240e | 3-ketoacyl-CoA thiolase, mitochondrial | AGACTGTGACCGCTATGC | TTCTTGAACACTGGAGGG |
| c154081.graph_c1 | 411.35 | 60.49 | 25.43 | 65.56 | 2.95 | up | 79 | K07508\|5e-08\|mmu:52538\|Acaa2, 0610011L04Rik, AI255831, AI265397, D18Ertd240e | 3-ketoacyl-CoA thiolase, mitochondrial-like, partial | – | – |
| c176818.graph_c0 | 290.24 | 72.69 | 6.12 | 28.94 | 2.15 | up | 942 | K00022\|0.0\|mmu:15107\|Hadh, AA409008, AU019341, AW742602, Hadhsc | hydroxyacyl-coenzyme A dehydrogenase, mitochondrial | GCCTCCATTTCTTCAACC | AACTTCATCGCCGTATCA |
| c189709.graph_c0 | 117.73 | 43.83 | 10.33 | 5.80 | 1.58 | up | 2292 | K07515\|0.0\|mmu:97212\|Hadha, C77020, Mtpa | trifunctional enzyme subunit alpha, mitochondrial | TGAAGGAAGTAGAAGGCGTGAC | TGGGAGCAAGACATCTGGTAG |
| c187908.graph_c0 | 11.82 | 34.23 | 3.70 | 3.48 | -1.38 | down | 921 | K01074\|0.0\|mmu:19063\|Ppt1, 9530043G02Rik, AA960502, C77813, CLN1, D4Ertd184e, INCL, MGC107420, PPT | palmitoyl-protein thioesterase 1 | TGGACCCTGTAGACTCTGA | ATGATGTGGGCATGAAAC |
| c186180.graph_c4 | 220.18 | 52.99 | 4.58 | 9.30 | 2.25 | up | 1356 | K01897\|0.0\|rno:94340\|Acsl5, Acs5, Facl5 | long-chain-fatty-acid–CoA ligase 5 isoform X1 | CCCTTTGATGATGAACTG | TAGGCTCTAGCAACCTGA |
| c166299.graph_c0 | 2319.63 | 90.17 | 3.68 | 78.44 | 4.86 | up | 2103 | K00232\|0.0\|mmu:80911\|Acox3, BI685180, EST-s59, PCOX | peroxisomal acyl-coenzyme A oxidase 3 isoform X1 | CCACTGGCTTGTCTGCTA | TTGCTCTTCCTGCTTGTT |
| c95056.graph_c0 | 11.97 | 36.63 | 6.38 | 6.80 | -1.52 | down | 1293 | K00255\|0.0\|mmu:11363\|Acadl, AA960361, AU018452, C79855, LCAD | long-chain specific acyl-CoA dehydrogenase, mitochondrial | TGATTGTAGTCGCCATAAC | TGAACTCACAGGCAGAAA |
| c177257.graph_c0 | 2.50 | 10.27 | 0.13 | 0.48 | -1.89 | down | 1299 | K09478\|0.0\|mmu:66885\|Acadsb, 1300003O09Rik, BB066609 | short/branched chain specific acyl-CoA dehydrogenase, mitochondrial isoform X2 | AATGGGTCAAAGATGTGG | TAACTGGCAGGTGGAAGA |
| c189754.graph_c0 | 96.29 | 34.81 | 1.48 | 19.50 | 1.66 | up | 870 | K13238\|1e-179\|rno:29740\|Dci | enoyl-CoA delta isomerase 1, mitochondrial isoform X1 | GCTGCCTCATAGCTCTTACC | ACCACCTCGTCCACCACA |
| c176790.graph_c0 | 1493.21 | 3.74 | 5.47 | 237.89 | 8.76 | up | 873 | K13239\|1e-159\|rno:291075\|Peci, MGC94706 | enoyl-CoA delta isomerase 2, mitochondrial | – | – |
| c186975.graph_c5 | 28.07 | 9.82 | 2.20 | 5.43 | 1.65 | up | 109 | K13239\|1e-18\|rno:291075\|Peci, MGC94706 | enoyl-CoA delta isomerase 2, mitochondrial | – | – |
| c184675.graph_c1 | 534.10 | 49.74 | 8.96 | 45.80 | 3.62 | up | 1434 | K00128\|0.0\|rno:65183\|Aldh3a2, Aldh4, FALDH | fatty aldehyde dehydrogenase | CCCCAACCATACTTACTGA | ACCCGTTTGATGACCTTA |

(Continued)

**Table S1 (continued).**

| #ID | Expression in secretion season | Expression in non-secretion season | STDEV of the secretion result | STDEV of the non-secretion result | log2FC | regulated | Length | KEGG_annotation | nr_annotation | Forward primer sequence (5'–3') | Reverse primer sequence (5'–3') |
|---|---|---|---|---|---|---|---|---|---|---|---|
| c166519.graph_c0 | 20.66 | 66.99 | 13.25 | 1.52 | -1.51 | down | 1560 | K00128\|0.0\|rno:29539\|Aldh2 | aldehyde dehydrogenase, mitochondrial isoform X1 | CCGTGTTCGGAGATGTGA | GCTTGGAGGGCTTGAGAC |
| c188162.graph_c0 | 37.22 | 130.67 | 55.05 | 8.26 | -1.63 | down | 1506 | K00128\|0.0\|mmu:11668\|Aldh1a1, Ahd-2, Ahd2, Aldh1, Aldh1a2, E1, Raldh1 | retinal dehydrogenase 1-like | TGGGAAGAAAGAAGGAGC | ACAGCCATAGCCAAATAG |
| c184362.graph_c0 | 66.09 | 19.33 | 4.60 | 5.46 | 1.97 | up | 1351 | K12408\|1e-173\|mmu:101502\|Hsd3b7, AI195443, BB098564 | 3 beta-hydroxysteroid dehydrogenase type 7 | GTGGACTTCGGCTGATAGG | TGGCGCTGTGCTTTGTTG |
| c154780.graph_c0 | 110.87 | 15.35 | 1.20 | 51.58 | 3.09 | up | 1149 | K01796\|0.0\|mmu:17117\|Amacr, Macr1 | alpha-methylacyl-CoA racemase | TGCTGGCGATTAAGGAGG | GTCTGGACTGAACCCAAACT |
| c179794.graph_c1 | 166.00 | 1.33 | 0.13 | 10.40 | 7.07 | up | 2115 | K10214\|0.0\|mmu:93732\|Acox2, THCCox | peroxisomal acyl-coenzyme A oxidase 2 | CTCTGTGACCTCTATGCCTTAC | GGAGACTTCTGAGCCCAAT |
| c188694.graph_c3 | 886.29 | 32.18 | 3.71 | 172.89 | 4.97 | up | 2208 | K12405\|0.0\|mmu:15488\|Hsd17b4, 17[b]-HSD, AW208803, MFE-2, MFP2, MPF-2, Mfp-2, perMFE-2 | peroxisomal multifunctional enzyme type 2 | TTTGCCAAGCCAGTGTATC | TTAAGGCGGCGACCTATC |
| c174928.graph_c0 | 5766.94 | 114.26 | 41.26 | 721.85 | 5.81 | up | 1641 | K08764\|0.0\|mmu:20280\|Scp2, AA409774, AA409893, C76618, C79031, NSL-TP, SCP-2, SCPx, ns-LTP | non-specific lipid-transfer protein | GCCAGGAAGTGCTATGAG | TGTCCCTTGGAAATGAGT |
| c189834.graph_c0 | 77.82 | 14.36 | 2.24 | 15.72 | 2.58 | up | 1026 | K01015\|0.0\|mmu:54200\|Sult2b1, AI326997, BB173635, ST2B1, SULT2B | sulfotransferase family cytosolic 2B member 1 | AGGCCAATACAATGTCCAA | GAGGGTTCTGGGTTAGGG |
| c149099.graph_c0 | 14.10 | 0.94 | 0.28 | 7.68 | 4.17 | up | 1539 | K00512\|0.0\|rno:25146\|Cyp17a1, Cyp17 | steroid 17-alpha-hydroxylase/17,20 lyase | CAAGCATTGGCGAGTTT | GGCACATCCAGGTCAAAC |
| c97465.graph_c0 | 131.82 | 21.25 | 6.54 | 18.10 | 2.77 | up | 876 | K00071\|1e-159\|rno:25116\|Hsd11b1, LRRGT00065 | corticosteroid 11-beta-dehydrogenase isozyme 1 isoform X2 | ATGGCAGCATTGTTGTCG | ACCCAGCTTGATATGTCGTAG |
| c179490.graph_c0 | 7.39 | 0.14 | 0.17 | 0.59 | 5.82 | up | 1549 | K07408\|0.0\|rno:24296\|Cyp1a1, AHH, AHRR, CP11, CYP1, Cyp45c, Cypc45c, P-450MC, P1-450, P450-C, P450DX | cytochrome P450 1A1-like | TGTCCTCCGCTACCTACC | GTCAAACCCTGCTCCAAA |
| c177279.graph_c0 | 1.35 | 6.86 | 2.58 | 0.26 | -2.16 | down | 996 | K12345\|0.0\|mmu:57357\|Srd5a3, 1110025P14Rik, A430076C09, AV364670, AW987574, D730040M03Rik, H5ar, S5AR_3, Srd5a2l | polyprenol reductase | ATAAGTGCCACGTCATTCTC | CTTTCCTATGCTTCGGGTA |
| c156542.graph_c0 | 8.04 | 30.47 | 2.91 | 5.72 | -1.83 | down | 1596 | K00699\|0.0\|mmu:94284\|Ugt1a6a, UDPGT_1-6, UGT1.6, Ugt1a6, Ugt1a7 | UDP-glucuronosyltransferase 1-1-like isoform X2 | CGAAGCCTATGTCAACGC | CATCATCACCATCGGCAC |
| c95502.graph_c0 | 15.91 | 6.38 | 0.67 | 1.57 | 1.51 | up | 1827 | K03846\|0.0\|mmu:102580\|Alg9, 8230402H15Rik, AI747665, B430313H07Rik, Dibd1 | alpha-1,2-mannosyltransferase ALG9 isoform 2 | TGGGCTCTTGTCATTCTC | CTCGGTTCTGGTCATTCA |
| c154819.graph_c0 | 51.98 | 18.61 | 3.54 | 7.00 | 1.68 | up | 1971 | K01230\|0.0\|rno:499751\|Man1b1, ERMan1, RGD1563595 | endoplasmic reticulum mannosyl-oligosaccharide 1,2-alpha-mannosidase | TACCAGATGAACCGACAGA | GTTGATAGAAGAATAGCCACC |
| c183448.graph_c0 | 96.44 | 29.95 | 3.86 | 13.11 | 1.86 | up | 1926 | K01230\|0.0\|rno:295319\|Man1a2, Man1b | mannosyl-oligosaccharide 1,2-alpha-mannosidase IB | AGCAGCACTGGCTATTGA | GTAACACGGGCAGAGGGT |

**Table S1 (continued).**

| #ID | Expression in secretion season | Expression in non-secretion season | STDEV of the secretion result | STDEV of the non-secretion result | log2FC | regulated | Length | KEGG_annotation | nr_annotation | Forward primer sequence (5'–3') | Reverse primer sequence (5'–3') |
|---|---|---|---|---|---|---|---|---|---|---|---|
| c182710.graph_c0 | 1.22 | 9.46 | 2.52 | 0.61 | -2.84 | down | 1848 | K01230\|0.0\|mmu:230815\|Man1c1, AI593348 | mannosyl-oligosaccharide 1,2-alpha-mannosidase IC | AAATCCGCAAGGTCCTCA | TCGCCACTCGGCAATGTA |
| c185766.graph_c0 | 4.62 | 20.35 | 1.36 | 2.90 | -2.02 | down | 1968 | K01230\|0.0\|ptr:463148\|MAN1A1 | mannosyl-oligosaccharide 1,2-alpha-mannosidase IA isoform X2 | GGGGACTAACATACATCGC | CACCATCAAATCGGAACG |
| c188645.graph_c0 | 3.12 | 8.77 | 1.09 | 0.84 | -1.34 | down | 3435 | K01231\|0.0\|mmu:17158\|Man2a1, Mana-2, Mana2, Map-2 | alpha-mannosidase 2 | AGACTGGGTGGTCGTGGAT | TGAGGCCCGTTCTTGTTC |
| c186296.graph_c0 | 4.21 | 15.32 | 5.52 | 1.19 | -1.71 | down | 1209 | K00778\|0.0\|rno:25197\|St6gal1, Siat1 | beta-galactoside alpha-2,6-sialyltransferase 1 isoform 1 | – | – |
| c166351.graph_c0 | 1091.24 | 243.19 | 29.20 | 239.77 | 2.35 | up | 1563 | K01641\|0.0\|ptr:461892\|HMGCS1 | hydroxymethylglutaryl-CoA synthase, cytoplasmic isoform X2 | GAAAGAGGGAAACGATAA | TCTGATTTGATACGAGCA |
| c119784.graph_c0 | 118.52 | 24.98 | 2.69 | 30.10 | 2.40 | up | 2664 | K00021\|0.0\|mmu:15357\|Hmgcr, HMG-CoAR, MGC103269, Red | 3-hydroxy-3-methylglutaryl-Coenzyme A reductase | AGTGGTGCGTCTTCCTCG | GCTTTCTCCGTGCCCTTG |
| c119745.graph_c0 | 100.34 | 12.58 | 1.02 | 49.48 | 3.17 | up | 1200 | K01597\|0.0\|rno:81726\|Mvd, Mvpd | diphosphomevalonate decarboxylase | CCGAGAAGAAGCAGATGGG | GGCAGGTGGCGTGAAACT |
| c178880.graph_c1 | 416.74 | 67.71 | 85.92 | 52.88 | 2.75 | up | 1005 | K11778\|0.0\|rno:298541\|Dhdds | dehydrodolichyl diphosphate syntase complex subunit DHDDS isoform X1 | CGGCTGAGTGACTTCTTAC | GTCTGTTCAAGCGTGTCC |
| c176644.graph_c0 | 29.25 | 3.82 | 0.33 | 10.29 | 3.15 | up | 1338 | K12505\|0.0\|rno:365592\|Pdss2 | decaprenyl-diphosphate synthase subunit 2 | CAGGACATGGCGTTTCAG | TTGAGCCTCACCAATCTG |
| c166709.graph_c0 | 81.81 | 15.25 | 4.88 | 1.86 | 2.42 | up | 1722 | K00511\|0.0\|mmu:20775\|Sqle, AI323792 | squalene monooxygenase | CCGTTGACTATTGTTGCA | GGTCAGGTATTTGTGGGTA |
| c148945.graph_c0 | 111.69 | 11.32 | 10.25 | 0.58 | 3.30 | up | 2196 | K01852\|0.0\|mmu:16987\|Lss, 2810025N20Rik, BC029082, D10Ertd116e, MGC27893, Osc | lanosterol synthase-like | TTTGAAGGCCGTGCTACT | GGGTCTCCCTGATTTCTACT |
| c142879.graph_c0 | 96.56 | 22.90 | 4.61 | 1.86 | 2.08 | up | – | K05917\|0.0\|rno:25427\|Cyp51, Cyp51a1, MGC93630, RATCP14DM | lanosterol 14-alpha demethylase-like | – | – |
| c147614.graph_c2 | 138.29 | 47.52 | 6.31 | 0.98 | 1.54 | up | 1191 | K01052\|0.0\|rno:25055\|Lipa, Chole, Chole2, LAL, Lip1 | lysosomal acid lipase/ cholesteryl ester hydrolase-like | TATGTGGCTTCAACGAGA | CTGGAGGGTAACTCTGGT |
| c172106.graph_c1 | 23.75 | 1.52 | 4.53 | 0.04 | 3.97 | up | 953 | K13373\|0.0\|rno:29540\|Hsd17b7 | 3-keto-steroid reductase isoform X2 | ATTCTGCCTCCCTTTGTG | AGCGGTGTCTTCATCTATGT |
| c154234.graph_c0 | 205.40 | 73.07 | 21.68 | 37.20 | 1.65 | up | 3306 | K01648\|0.0\|mmu:104112\|Acly, A730098H14Rik, AW538652 | ATP-citrate synthase isoform X4 | TCTGTGCTCGGGCTGGAA | ACTTCCAGGGCGTAATCG |
| c181718.graph_c0 | 105.12 | 49.04 | 8.44 | 4.68 | 1.27 | up | 2670 | K01681\|0.0\|mmu:11428\|Aco1, AI256519, Aco-1, Irebp, Irp1 | cytoplasmic aconitate hydratase isoform X1 | GTGGAACGGCAGTATGTC | CTCTGTTGGTCAAGTAGCG |
| c184117.graph_c2 | 398.94 | 92.98 | 22.46 | 31.59 | 2.30 | up | 1245 | K00031\|0.0\|rno:24479\|Idh1 | isocitrate dehydrogenase [NADP] cytoplasmic | TGGGCGTTTCAAAGACAT | ATGCCAAGGGAACCGTAA |

(Continued)

**Table S1 (continued).**

| #ID | Expression in secretion season | Expression in non-secretion season | STDEV of the secretion result | STDEV of the non-secretion result | log2FC | regulated | Length | KEGG_annotation | nr_annotation | Forward primer sequence (5'–3') | Reverse primer sequence (5'–3') |
|---|---|---|---|---|---|---|---|---|---|---|---|
| c189729.graph_c0 | 116.86 | 53.73 | 16.80 | 4.00 | 1.30 | up | 1158 | K00030\|0.0\|rno:94173\|Idh3B, MGC94111 | isocitrate dehydrogenase [NAD] subunit beta, mitochondrial isoformX1 | TGTGAGGAAGTCGCTGAA | TGTAGCCGCCCATGTCTCG |
| c154485.graph_c0 | 53.07 | 23.39 | 3.65 | 2.68 | 1.35 | up | 1392 | K01900\|0.0\|mmu:20916\|Sucla2, 4930547K18Rik | succinyl-CoA ligase [ADP-forming] subunit beta, mitochondrial isoform X1 | TAGAAGGCATCAGGAAGG | AACCCAGCACCATTTACT |
| c187137.graph_c0 | 140.46 | 53.21 | 22.63 | 11.32 | 1.53 | up | 996 | K01054\|0.0\|rno:29254\|Mgll, MAGL, MGC124942 | monoglyceride lipase isoform X3 | TGCCAAAGTGCTCAACCT | ATGGAGGACAGAGTTGGTGA |
| c185154.graph_c1 | 83.19 | 5.37 | 8.52 | 3.92 | 4.14 | up | 1178 | K13534\|1e-180\|mmu:116939\|Pnpla3, Adpn | patatin-like phospholipase domain-containing protein 3 isoform X4 | TTCAAGGCTACCTGGACG | CCTCAGATAGCCGTCCCT |
| c180403.graph_c0 | 49.98 | 18.88 | 9.49 | 1.79 | 1.61 | up | 1732 | K11155\|0.0\|mcc:701489\|DGAT1 | diacylglycerol O-acyltransferase 1 | CCCACTGACTTTCTTCCC | CCATGCCTGATTATTGCA |